Order Number 9114276

Magnetic resonance characterization of gadolinium-based contrast agents

Hwang, Jong-Hee, Ph.D.

University of Illinois at Urbana-Champaign, 1990

U·M·I
300 N. Zeeb Rd.
Ann Arbor, MI 48106

MAGNETIC RESONANCE CHARACTERIZATION OF GADOLINIUM-BASED CONTRAST AGENTS

BY

JONG HEE HWANG

B.Eng., Yonsei University, Seoul, 1979
M.S., Yonsei University, Seoul, 1983

THESIS

Submitted in partial fulfillment of the requirements
for the degree of Doctor of Philosophy in Chemistry
in the Graduate College of the
University of Illinois at Urbana-Champaign, 1990

Urbana, Illinois

UNIVERSITY OF ILLINOIS AT URBANA-CHAMPAIGN

THE GRADUATE COLLEGE

SEMTEMBER 1990

WE HEREBY RECOMMEND THAT THE THESIS BY

JONG HEE HWANG

ENTITLED MAGNETIC RESONANCE CHARACTERIZATION OF GADOLINIUM-BASED CONTRAST AGENTS

BE ACCEPTED IN PARTIAL FULFILLMENT OF THE REQUIREMENTS FOR

THE DEGREE OF DOCTOR OF PHILOSOPHY

A. Lynn Belford
Director of Thesis Research

Head of Department

Committee on Final Examination†

A. Lynn Belford
Chairperson

Paul C. Lauterbur

W.S. Brey

RB Clarkson

† Required for doctor's degree but not for master's

O-517

Acknowledgement

I would like to thank to all who have helped me in making this thesis possible. Especially my advisors, Dr. Belford and Dr. Clarkson, deserve credit not only for scientific guidance, but also for the encouragement for last several years.

I have appreciated the encouragement and help from all the group members of my research group. I also thank S. Frank for his help in the relaxometer work.

I really thank to my family who always support me, and many precious friends here, and back in Korea.

Thank you all.

TABLE OF CONTENTS

CHAPTER 1

Introduction to Contrast Agents in Magnetic Resonance Imaging and the Related Basic Theory

1.1 Background

This chapter will provide an introductory description of contrast agents in NMR Imaging and the related basic theory. Nuclear Magnetic Resonance experiments have started in the 1940's, and Lauterbur introduced Magnetic Resonance Imaging (MRI) in 1973.[1] That was one of the early applications of NMR to medical science. As a diagnostic technology, MRI has become popular and powerful in observing the brain, neck, spine, and other parts. The development of MRI has created a whole new class of pharmaceuticals, contrast agents for MRI. In 1984, D.H. Carr and Schering-AG observed the big contrast between normal and tumor cells enhanced by Gd DTPA (Diethylenetriaminepentaacetic acid), which was intravenously injected into patients with brain tumors.[2] This compound is the only contrast agent in MRI approved by the FDA as of today. These applications of contrast agents have made MRI more useful for diagnostic purposes. Many papers have been written on developing and improving contrast agents; some of the papers cover various areas including synthetic chemistry, physical chemistry and medical science. The characterization of Gd-

based contrast agents by several magnetic resonance methods will be discussed in this thesis.

1.2 Aim of This Study

As we review the brief history of contrast agents in MRI, we point out that it is still at an early stage. Several research groups are working on contrast agents in many different ways. Here we investigate contrast agents by the combination of EPR and NMR. This was rarely attempted before. Paramagnetic contrast agents are a very good substance for EPR studies because of their nature. Compared to NMR, the EPR method has an advantage in that it can look at the paramagnetic center selectively. The results obtained by the EPR method can give useful information that can otherwise not be obtained by NMR. These two methods sometimes complement each other. For the paramagnetic contrast agents study, it is thought that both of these methods are needed, because what we observe is nuclear relaxation enhanced by paramagnetic materials.

In this thesis, several magnetic methods are introduced. There is no doubt, the relaxometer is very useful for measuring relaxation rates at various magnetic fields. However, the analysis of the NMRD curves sometimes include some ambiguities because there are many parameters to control in the simple NMRD curves. To make relaxation data more useful, and to get a clear picture of the relaxation enhancing phenomena, more reliable data should be taken as separately as possible by various magnetic resonance methods. Without this information from other techniques, it is very difficult to set the strategy to control the factors for relaxivity of contrast agents. On the basis of this idea, all results will be analyzed by combining results from several different methods. The plan for this study is in figure 1.1.

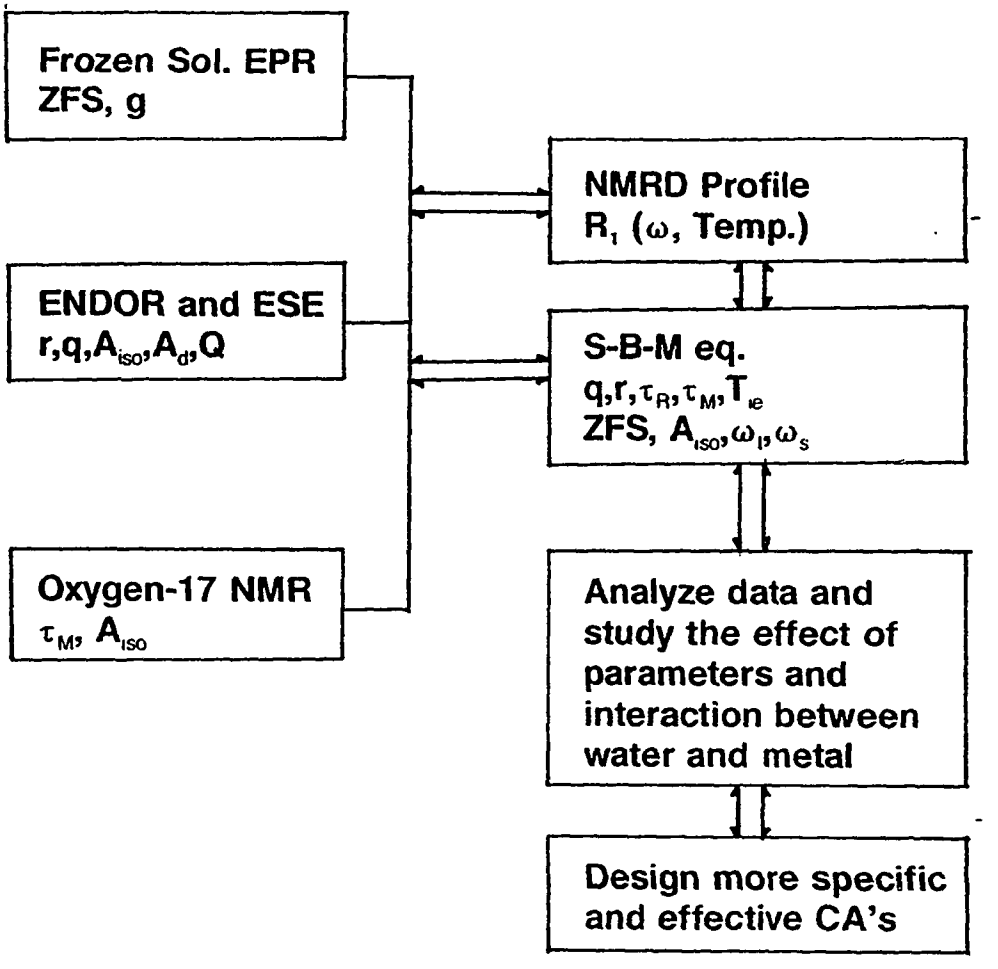

Figure 1.1. The map of research planning for this study

It explains how each parameter is measured by a certain method separately or in a combined fashion. Finally we utilize all results to understand the relaxation enhancing effect on a molecular level, and eventually help the designing of paramagnetic contrast agents become more effective and more specific.

1.3 Material Aspect of Paramagnetic Contrast Agents[3)]

1.3.1 General Substances of Paramagnetic Contrast Agents

Various paramagnetic materials can be used for paramagnetic contrast agents, such as the transition metal complexes of Mn^{+2}, Fe^{+3}, and Cr^{+3} with the ligands. Iron oxide materials are also used as contrast agents, which show superparamagnetism or ferromagnetism depending upon the size of the particles. For the case of free radicals, the nitroxide free radical is also studied as a contrast agent. In this study only Gd^{3+} complexes will be discussed.

1.3.2 The Advantages of Gd Complexes as Contrast Agents

The electronic configuration of Gd^{3+} is $4f^7$, which has seven unpaired electrons, thereby allowing it to create a big magnetic moment. In general, lanthanide metals have very short electronic relaxation times, but Gd^{3+} has a relatively long relaxation time ($\sim 10^{-9}$ sec) to see the paramagnetic enhancing effect because of a very stable ground state, $^8S_{7/2}$. Free Gd^{+3} and organic ligands are toxic individually; however, Gd^{3+} shows great affinity to the organic ligands and form stable complexes. That stability increases the safety as a contrast

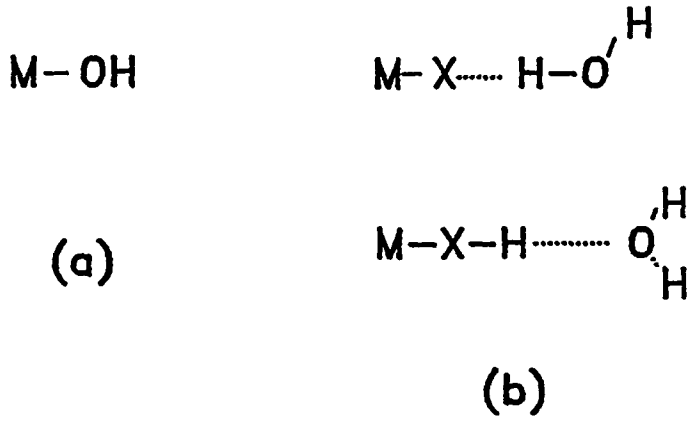

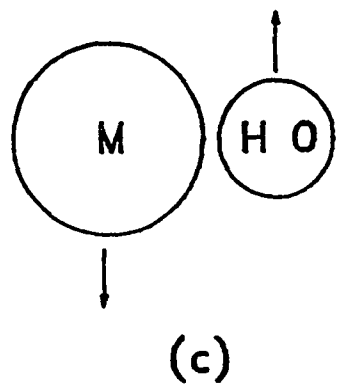

Figure 1.2. Inner and outer sphere water

a) inner sphere water

b) second sphere water

c) outer sphere water

agent.

1.3.3 Contributions to Proton Relaxation Enhancing by Paramagnetic Contrast Agents

The relaxation rates observed after adding the paramagnetic contrast agents equal the total relaxation rates of the paramagnetic and the diamagnetic part. Those will be discussed in detail in section 1.5. Paramagnetic contribution is divided into inner sphere and outer sphere contributions. One usually classifies water molecules by the interactions between the water and the paramagnetic metal center. Inner sphere water is a water that has a direct bond with metal. Outer sphere water can be differentiated by some bond between the complex and has no chemical bond at all as indicated in figure 1.2. The former is usually termed "second sphere water".

1.4 Theoretical Aspect of Paramagnetic Contrast Agents

1.4.1 General Concept[4), 5), 6)]

In water, water protons relax through the fluctuating nuclear dipole fields. In the absence of paramagnetic species, this dipole relaxation is not efficient enough and they relax quite slowly. Adding paramagnetic impurities greatly affects the nuclear relaxation rate of bulk water. The electron in paramagnetic materials provides a reservoir to a nuclei for relaxing energy. Providing one more relaxation pathway to protons of water results in the expedition of proton relaxation. That is called proton relaxation enhancing by the paramagnetic metal. Whatever the mechanisms for explaining this phenomenon are, the most

important fact is that it is concerned with the interaction between the nuclei and the electron. In this section, an introductory basic theory between I and S interaction, and Solomon-Bloembergen equations will be discussed.

1.4.2 Interaction Involving the Electron Spin

The important hyperfine interactions for nuclei are from electric or magnetic interaction. The electric hyperfine interaction is the electric quadrupole moment of the I > 1/2 nucleus and the fields gradient at the site of the nucleus. The magnetic hyperfine interaction is that the interaction between the nucleus and electronic magnetic moment. In order to study the system of water containing the paramagnetic impurities, the most important hyperfine interaction that we are interested in is the magnetic interaction. The nuclei we are concerned with are mostly water protons, therefore I = 1/2. Thus quadrupole interaction is less important. The hyperfine Hamiltonian from this interaction is usually described as ,

$$\mathcal{H}_h = 2\beta\gamma h [\, \hat{I}\bullet(L - \hat{S})/r^3 + 3(\hat{I}\bullet\vec{r})(\hat{S}\bullet\vec{r})/r^5 + 8\pi/3\, \delta(\vec{r})\hat{I}\bullet\hat{S}]\mu_o/4\pi, \qquad [1.1]$$

where ß = eh/2me is the Bohr magneton. The first two terms within square brackets describe the interaction between the nuclear magnetic moment at the electron outside of the nucleus(the dipole-dipole interaction). The last term represents the interaction with the s-electron at the site of the nucleus(the contact interaction). If we neglect L, equation 1.1 becomes,

$$\mathcal{H}_h = \hat{I}\bullet\overleftrightarrow{A}\bullet\hat{S}$$

$$\overleftrightarrow{A} = 2\beta\gamma h\mu_o/4\pi[-1/r^3 + 3\vec{r}\,\vec{r}/r^5 + 8\pi/3\delta(\vec{r})]. \qquad [1.2]$$

1.4.3 The Spin Hamiltonian

The spin Hamiltonian for the system which we are interested in is ,

$$\mathcal{H}_s = \hat{S}\cdot\overleftrightarrow{g}\cdot\vec{B}_o + \hat{S}\cdot\overleftrightarrow{D}\cdot\hat{S} + \hat{I}\cdot\overleftrightarrow{A}\cdot\hat{S}. \qquad [1.3]$$

where the first term is Zeeman, the second one is zero field splitting, and the last term is the electron- nuclear hyperfine term.

1.4.4 The Origin of Magnetic Relaxation

The basic equations for magnetic relaxation of NMR are Block equations. These equations taught us that the two relaxation times play different roles in the case of non-interaction with a reservoir. T_1 (longitudinal or spin-lattice) relaxation time determines the degree of saturation and T_2 determines the unsaturated line width. Both relaxations are caused by time dependent magnetic or electric fields at the nucleus (or the electron). These fields in turn form the random thermal motion which is present in any form of matter. A nuclear spin of 1/2, for example, may experience local magnetic fields from the spins of other nuclei moving from unpaired electrons, or from spin rotational interaction in which the molecular rotation itself generates magnetic fields at the nuclei. Nuclei with electric quadrupole moments are farther affected from other electrons of nuclei. In particular radicals with an anisotropic g tensor experience fluctuating Zeeman interactions with the external magnetic field, which can be a powerful means of relaxation.

In general, two conditions are necessary for a successful relaxation mechanism. First, there must be some interaction which acts directly on the spins. Secondly that interaction

must be time dependent. An essential requirement for relaxation is that the molecular motion has a suitable time scale. Interactions which change sign at a rate much faster than the magnetic resonance frequency (10^{10} cps for electrons or,10^{7} cps for nuclei) have little effect. Thus electronic motions and molecular vibrations are related. Any interaction which causes the transition between two $m_I = 1/2$ and $m_I = -1/2$ spin states and fluctuates strongly at the resonance frequency and produces powerful spin lattice relaxation and line broadening. Another cause of interaction modulates the spin energy levels at low frequency without causing transition between the two states. For relaxation in liquid , rotation and diffusion motion are very important. Here most of the effects arise from random Brownian motion of the molecules as they rotate and diffuse through the fluid. The theory is simple and satisfactory. The subject of relaxation in liquids is extensive and complicated; thus, the description of rotation and diffusion motions are not discussed here.

1.4.5 Short and Long Correlation Time

The rapid motion of liquid covers a wide spectrum and it is necessary to measure the frequency distributions and their strength. If a function, F(t), is some random force and it fluctuates about a mean value of zero, one can measure the strength of the mean square average by $F^{*}(t)F(t)$. The correlation function of F(t) is defined as the average value of the product of F(t) and $F^{*}(t + \tau)$.

$$G(\tau) = F^{*}(t + \tau) \cdot F(t) \qquad [1.5]$$

$G(\tau)$ is large for a short amount of time, and it dies away to zero exponentially, as τ increases.

$$G(\tau) = F^{*}(t)F(t)\, e^{-|\tau|/\tau c} \qquad [1.6]$$

where τ_c is called correlation time. If we want the Fourier transform of the correlation function, it can be written as,

$$J(\omega) = \int_{-\infty}^{\infty} G(\tau)\, e^{i\omega\tau} d\omega \qquad [1.7]$$

with inverse relation and the case of the transition from m to k state,

$$G_{mk}(\tau) = 1/2\pi \int_{-\infty}^{\infty} J_{mk}(\omega)\, e^{i\omega\tau}\, d\omega \qquad [1.8]$$

$$G_{mk}(0) = (m|\mathcal{H}_1(t)|k)^2 = 1/2\pi \int_{-\infty}^{\infty} J_{mk}(\omega)\, d\omega. \qquad [1.9]$$

This tells us the area of the spectral density curve remains fixed as τ_c varies. These three curves of $J_{mk}(\omega)$ for three different τ_c are shown in figure 1.3 (a). As τ_c varies, the total area of three curves remains the same. If the energy difference m - k were equal to the value ω_1, the spectral density $J_{mk}(\omega_1)$ of the curve of median τ_c would be the greatest of the three at the frequency ω_1. The correlation time and the longitudinal relaxation time is in figure 1.3 (b).

1.4.6 Solomon-Bloembergen-Morgan equations and Relaxation by Paramagnetic Ions in Solution[7),8),9),10)]

The most important two factors for relaxation enhancing by paramagnetic species are,

1) Large local field by the electrons (~ 1000 times greater than nuclei)

2) Short electron spin relaxation times (~ 10^{-9} - ~10^{-12}).

B_{eff} fluctuates rapidly and induces fast transitions between the nuclear spin states. If the nuclei spins are in the immobile state as in a solid, then little effect is generated by

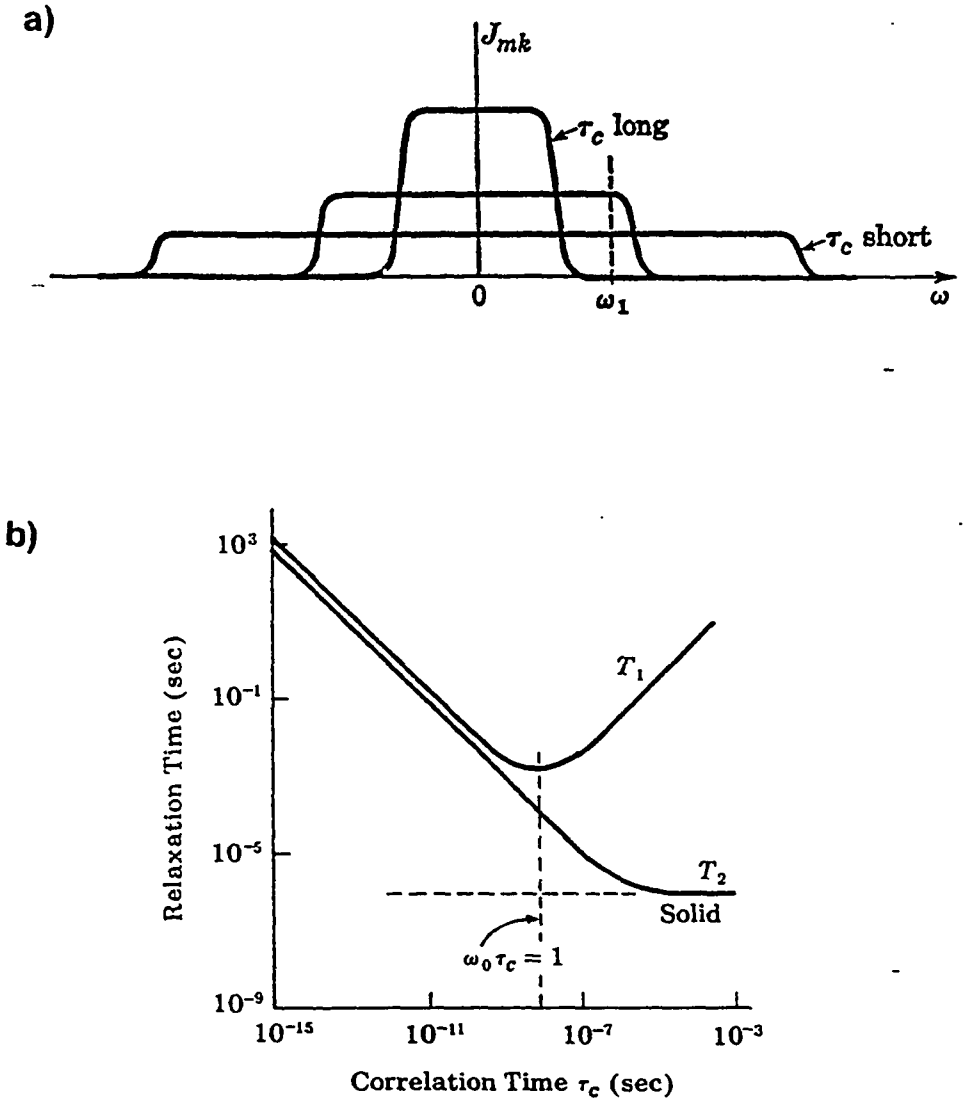

Figure 1.3. (a) J_{mk} for three values of correlation time. (taken from ref. 4.)

(b) Theoretical behavior of T_1 and T_2 as a function of correlation time. (taken from ref. 5.)

paramagnetic impurities. The basic rule is that $1/T_1$ and $1/T_2$ are proportional to the concentration of paramagnetic materials in the water and to the effective magnetic moments which are generated by the paramagnetic metals.

$$1/T_1 = (1\text{-}f)/T_{1a} + f/T_{1M} \qquad [1.9]$$

where T_{1a} is the longitudinal relaxation time of bulk water and T_{1M} is that of water which was coordinated to water.

$$1/T_2 = (1\text{-}f)/T_{2a} + f/T_{2M} \qquad [1.10]$$

where subscript '2' means transverse relaxation times. In general, relaxation times of proton water are enhanced by coordination to the paramagnetic metal through dipolar coupling and scalar coupling. Scalar hyperfine interaction is,

$$\mathcal{H}(t) = a(t)\hat{S}_z(t)\,\hat{I}_z, \qquad [1.11]$$

which emphasizes that the electron spin undergoes fast relaxation.

$$1/\tau_{ei} = 1/\tau_M + 1/T_{ie} \qquad [1.12]$$

$$\begin{aligned} <\hat{S}_z(t+\tau)\cdot\hat{S}_z(t)> &= <\hat{S}_z^2> \exp(-\tau/T_{1e}) \\ &= 1/3S(S+1)\exp(-\tau/T_{1e}) \end{aligned} \qquad [1.13]$$

where T_{1e} is the electron spin relaxation time. However, a proton stays at a given electron for a limited time, τ_M, and so the correlated function decays away with a further exponential functions, $\exp(-\tau/T_{1e})$. The effective lifetime of electron spins is therefore given by the following exponent.

$$\begin{aligned} <\hat{S}_z(t+\tau)\hat{S}_z(t)> &= 1/3\ S(S+1)\ \exp(-\tau/T_{1e})\cdot\exp(\tau/\tau_M) \\ &= 1/3S(S+1)\ \exp(-\tau/\tau_{e1}) \end{aligned} \qquad [1.14]$$

For dipolar interaction, rotational motion is also important, because it contains angular

dependency. The S-B-M equations are as follows.

$$1/\tau_{ci} = 1/\tau_R + 1/\tau_M + 1/T_{ie} \qquad i=1,2 \qquad [1.15]$$

$$1/\tau_{ei} = 1/\tau_M + 1/T_{ie}$$

$$\frac{1}{T_{1M}} = \frac{2}{15}\frac{\gamma_I^2 g^2 S(S+1)\beta^2}{r^6}\left(\frac{7\tau_{C2}}{1+\omega_S^2\tau_{C2}^2} + \frac{3\tau_{C1}}{1+\omega_I^2\tau_{C1}^2}\right)$$

$$+ \frac{2}{3}S(S+1)\left(\frac{A}{h}\right)^2\left(\frac{\tau_{e2}}{1+\omega_S^2\tau_{e2}^2}\right) \qquad [1.16]$$

$$\frac{1}{T_{2M}} = \frac{1}{15}\frac{\gamma_I^2 g^2 S(S+1)\beta^2}{r^6}\left(\frac{7\tau_{C2}}{1+\omega_S^2\tau_{C2}^2} + \frac{13\tau_{C1}}{1+\omega_I^2\tau_{C1}^2} + 4\tau_{c1}\right)$$

$$+ \frac{1}{3}S(S+1)\left(\frac{A}{h}\right)^2\left(\frac{\tau_{e2}}{1+\omega_S^2\tau_{e2}^2} + \tau_{e1}\right) \qquad [1.17]$$

1.4.7 Electron Spin Relaxation Effects[11]

The original Solomon-Bloembergen equations did not consider electronic relaxation in detail. Later Bloembergen and Morgan included the electron spin relaxation time in the extreme narrowing regime. The following averaged values were calculated by McLachlan for S = 7/2:

$$\frac{1}{T_{1e}} = \left(\frac{6}{5}\right)\left(\frac{2D^2}{3} + 2E^2\right)\left(\frac{2\tau_V}{1 + \omega_S^2\tau_V^2} + \frac{8\tau_V}{1 + 4\omega_S^2\tau_V^2}\right) \qquad [1.18]$$

$$\frac{1}{T_{2e}} = \left(\frac{6}{5}\right)\left(\frac{2D^2}{3} + 2E^2\right)\left(3\tau_V + \frac{5\tau_V}{1 + \omega_S^2\tau_V^2} + \frac{2\tau_V}{1 + 4\omega_S^2\tau_V^2}\right) \qquad [1.19]$$

1.4.8 Koenig's Modified Solomon-Bloembergen-Morgan equations.[12]

Koenig modified the basic McLachlan's averaged electronic relaxation time using his own method, deleting zero-field splitting parameters. Koenig's modified equation is,

$$\frac{1}{T_{1e}} = \frac{0.2}{\tau_{SO}}\left(\frac{1}{1 + \omega_S^2\tau_V^2} + \frac{4}{1 + 4\omega_S^2\tau_V^2}\right) \qquad [1.20]$$

Therefore the averaged zero field aplittting value and Koenig's τ_{SO} are related as follows.

$$\tau_V\left(\frac{12}{5}\right)\left(\frac{D^2}{3} + E^2\right) = \frac{0.2}{\tau_{SO}}$$

$$\therefore \tau_{SO} = 0.2 \times \left(\frac{5}{12}\right)\left[(\tau_V)\left(\frac{D^2}{3} + E^2\right)\right]^{-1} \qquad [1.21]$$

The unique point of his approach is that the zero field splitting is the product of τ_V. Therefore, he deals a zero field splitting energy which can vary according to the temperature and the state of solutions, because τ_V is dependent on η/T.

1.4.9. The Limits of Solomon-Bloembergen-Morgan Equations

The Solomon-Bloembergen-Morgan (S-B-M) equations include the Redfield theory in the nuclear system. Therefore, the assumptions in the Redfield theory are also applied to the S-B-M equations. Apart from limits of the Redfield theory, the following assumptions are also included in the S-B-M equations.

i) The electron spin is assumed to be a point-dipole centered at the metal center.

ii) The electron g tensor is assumed to be isotropic.

iii) The orientational correlation function for the nuclear-electron spin vector is assumed to be the exponential decay with single correlational time.

iv) It is assumed that chemical exchange is unrelated to the remaining motion in the lattice.

v) It is assumed the Redfield limit is applied for the electron spin relaxation.

vi) The electron spin relaxation is characterized by a single exponential decay.

vii) The motions in the electron spin system are assumed to be unrelated to the motions in the remaining part of lattice.

Rather than using point-dipole approximation, Kowalevski et.al. treated electron-nuclear interaction by using a spatial distribution of electron spin density, which can be applied to general situations. But here the Kowalevski method will not be dicussed, because we found several results that support the S-B-M equations for the Gd^{3+} system, which will be discussed in later chapters. Only the S-B-M equations are discussed here .

1.5 Overall Contributions to Relaxivity by Paramagnetic Contrast Agents

The total observed relaxation rate is a combination of the diamagnetic and paramagnetic contributions.

$$(1/T_i)_{obs} = (1/T_i)_{dia} + (1/T_i)_{para} \qquad \text{where } i = 1 \text{ or } 2 \qquad [1.22]$$

The paramagnetic part can be expressed in another way,

$$(1/T_i)_{obs} = (1/T_i)_{dia} + R_i[M] \qquad [1.23]$$

Where R_i is termed as relaxivity of longitudinal or transverse axis, and [M] stands for the concentration of the paramagnetic species added. Thus R_i is expressed in the units of $[mM \cdot sec]^{-1}$ or $[M \cdot sec]^{-1}$.

Paramagnetic contribution is divided into inner sphere and outer sphere contributions.

$$(1/T_i)_{para} = R_i[M] = (1/T_i)_{inner} + (1/T_i)_{outer} \qquad [1.24]$$

We need another theory besides the Solomon-Bloembergen model to explain outer sphere relaxation. The inner sphere water relaxation rate is expressed in the following equation.

$$(1/T_i)_{inner} = P_M q/(\tau_M + T_{1M}) \qquad [1.25]$$

where q is the number of inner sphere water, P_M is a mole fraction of paramagnetic species, τ_M is the exchange correlation time, and the T_{1M} is the relaxation rate of a water proton directly bound to the metal, which can be calculated by S-B-M equations.(equations 1.15-1.18).

So far, several parameters have been mentioned. Each will be briefly reviewed in the next section. The application of each parameter to real Gd^{3+} systems will be discussed in detail in chapter 5.

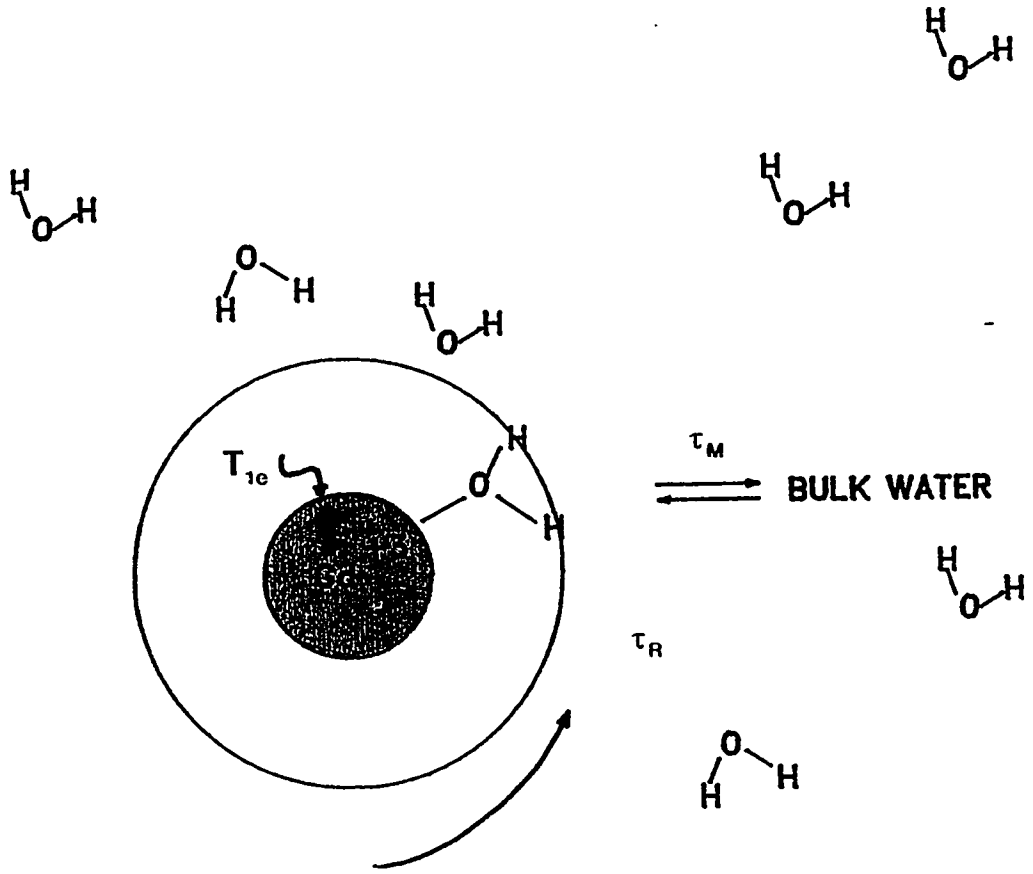

Figure 1.4. Illustration of T_{1e}, and τ_M, and τ_R

1.5.1 q and r

The number of inner sphere water, q, and the distance between the metal center and the proton of inner sphere water greatly affects the relaxation enhancing effect. According to the S-B-M model, the relaxation rate of a proton attached to the metal is proportional to $(1/r^6)$. Thus the accurate structural information of these Gd^{3+} molecules is one of major concerns of this study.

1.5.2 τ_R and Molecular Weight

The rotational correlation time, τ_R is in the unit of pico seconds. As the total correlation time is the sum of the inverse of τ_R, τ_M, and T_{1e}, usually the shortest one, τ_R, dominates the total correlation time. The τ_R is directly related to the size of molecules. One can increase the relaxivity by increasing the size of the molecule. When paramagnetic molecules are bound to larger molecules such as proteins, relaxation enhancing is observed. Often this is called Proton Relaxation Enhancing Effect (PRE effect).

1.5.3 τ_M

The exchange correlation time, τ_M, is important in two aspects. It plays a role in equation 1.25, and also its contribution to the total correlation time(equation 1.15). As it is in units of nano seconds, its contribution to the total correlation time for the small molcule case is not prominent.

1.5.4 τ_{SO},τ_v, T_{1e}, and zero field splitting constant

All these parameters are related to the electron spin relaxation effect. Koenig uses

τ_{SO} in equation 1.18 for calculating the average value of T_{1e} instead of zero field splitting. The zero field correlation time, τ_v, is related to vibrational or wedging motions of the ligand atoms attached to the central metal. It is usually one to ten pico seconds in water solution at room temperature. It is dependent upon η/T, where η is the viscosity constant of the solvent. For Gd^{3+} complexes, zero field splitting constants are found to be small (0 - 2,000 MHz). That results in the longer T_{1e}, normally a nano second unit or close to it.

REFERENCES

1. Lauterbur,P.C.,Nature, **1973**, 242, 190

2. Carr, D.H.;Brown,J; Bydder,G.M.; Weinmann,H.-J.;Speck,U.;Thomas,D.J.; Young, I.R., Lancet, **1984**, 1, 484

3. Lauffer, R.B. Chem. Rev., **1987**, 87, 901

4. Slichter,C.P.,"Principles of Magnetic Resonance",1990, Springer-Verlag, Berlin Heidelberg

5. Carrington,D.;McLachlan,A.D., "Introduction to Magnetic Resonance", 1980, Chapman and Hall, New York

6. Kowalevski,J.; Nordenskiold,L.; Benetis, N.; Wesrlund,P.-O., Prog. NMR Spectr. **1985**, 17, 141

7. Solomon,I.; Phys. Rev., **1955**, 31, 365

8. Morgan, L.O.; Nolle,A.W., J. Chem. Phys., **1959**, 31, 365

9. Bloembergen,N.; Morgan, L.O., J. Chem. Phys., **1961**, 34, 842

10. Reuben, J.; Redd, G.H.; Cohn,M., J. Chem. Phys., **1970**, 52, 1917

11. McLachlan, A.D.,Pro. R. Soc., **1964**, A280, 271

12. Koenig, S.H.; Epstein, M., J. Chem. Phys., **1975**, 63, 2279

CHAPTER 2

EPR Studies of Gd-based Contrast Agents

2.1 Background

The phenomenon of proton relaxation enhancement by paramagnetic metals is not yet clearly understood. In order to understand it better, more fundamental information which can be obtained by EPR and NMR is needed. Here we report the EPR studies of Gd^{3+} with several polyamino polycarboxylic ligands including Gd (DTPA)$^{-}$.

The contrast of MRI can be controlled by changing T_1 (longitudinal relaxation time) and T_2 (transverse relaxation time). These relaxation times of water protons are shortened by small impurities of paramagnetic metals mainly by the dipolar interaction between the electron of the metal and proton of water. This is called Proton Relaxation Enhancement (PRE) by paramagnetic metals. Gd^{3+} has advantages for this effect because it has seven unpaired electrons ($4f^7$), that result in a large magnetic moment. Therefore it can create a larger effect on the water protons. Often this PRE effect can be quantitatively calculated by the Solomon-Bloembergen-Morgan equations.[1),2),3)] But those equations are valid under the several assumptions such as, strong narrowing regime and electronically non-distorted model. Thus

the results of EPR studies of Gd^{3+} will also help the determination of the applicability of Solomon-Bloembergen-Morgan equations to Gd^{3+} systems.

Here we report the EPR simulation results of Gd^{3+} for a series of polyamino polycarboxylic ligands. The ligands in figure 2.1 with Gd^{3+} systems are examined.

2.2 Theory

2.2.1 Spin Hamiltonian

EPR spectra of Gd^{3+} in oxide glasses, which is often referred to "U" type spectra, indicate low site symmetry with a broad distribution of crystal field. The origin of the spectrum has been discussed by several authors,[4), 5), 6)] and was thoroughly treated by Brodbeck and Iton with Gd^{+3} in silica glasses.[7)] We are employing basically the same methods for simulating the EPR spectra of Gd^{+3} complexes with organic ligands.

The spin hamiltonian for Gd^{3+} can be written in terms of operators O_n^m as defined by Abragam and Bleaney.[8)]

$$\mathcal{H} = g_0 \beta H S + \Sigma \Sigma B_n^m O_n^m. \qquad [2.1]$$

According to Brodbeck and Iton, only $n=2$, second degree terms are allowed and often have a dominant effect on the energy levels. The simplified spin hamiltonian is following.

$$\mathcal{H} = g_0 \beta H S + 1/3(b_2^0 O_2^0 + b_2^2 O_2^2) \qquad [2.2]$$

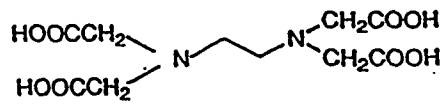

EDTA

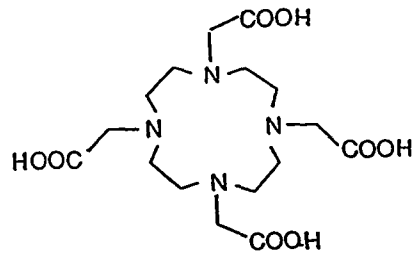

DOTA

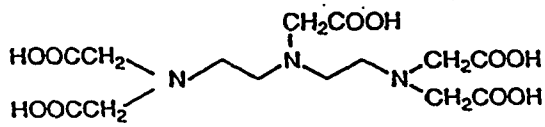

DTPA

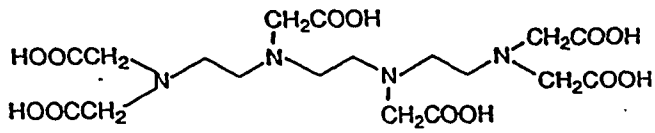

TTHA

Figure 2.1 Structures of Ligands

DTPA (diethylenetriaminepentaacetic acid)

EDTA (ehtylenediaminetetraacetic acid)

TTHA (triethylenetetraaminehexaacetic acid)

DOTA (1,4,7,10-tetraazacyclododecane-N,N',N'',N'''-tetraacetic acid)

If we convert this equation to familiar terms D and E,

$$\mathcal{H} = g_o \beta H S + D(S_z^2 - 1/3S(S + 1)] + E (S_x^2 - S_y^2) \qquad [2.3]$$

When the Zeeman term is small compared with crystal-field, which is called strong the crystal field region, EPR will be seen only between Kramers-conjugated states providing prominent features at certain well defined g-values. When the Zeeman term is larger than the crystal field term, EPR transitions will be concentrated close to $g = g_o \approx 2$, corresponding to the selection rule $\Delta M_s = \pm 1$, usually called the weak crystal field region. As Brodbeck and Iton pointed out, a distribution of D and E values gives a better fit for the simulations of EPR spectra of Gd^{3+} chelates compounds.

2.3 Experimental

2.3.1 Chelating Structures and pH Dependence of Gd^{3+} in Aqueous Solution

The structures of Gd^{3+} complexes with multidentate organic ligands show strong pH dependence.[9] In low pH, the equilibrium is shifted to the dissociation of ligands and Gd^{3+} metals. For the study of contrast agents, having the water and the ligand binding to Gd^{3+} is very important, therefore all experiments were done in the neutral pH range of 6-7. Another reason for keeping this pH range is mimicking the environment close to physiological pH = 7.4 of the human body.

2.3.2 Choice of Glasses

In order to perform the EPR experiment in frozen glasses similar to the environment

of water, water/methanol or water/glycerol glasses were chosen for this experiment.

2.3.3 EPR Measurements

Three millimolar concentration solutions of Gd(DTPA) megl (meglumine), Gd(EDTA) megl, Gd(TTHA) Na_3 and Gd(DOTA) Na were prepared in water/methanol. All Gd complexes were synthesized by Schering-AG, Berlin. EPR measurements were done with an X-band Bruker EPR spectrometer at liquid nitrogen temperature at the Illinois EPR Research Center at the University of Illinois.

2.4 Simulations

Each EPR spectrum was simulated with a Fortran program developed in our laboratory based on equation 2.3 in the theory section. As in Brodbeck's paper,[7] the exact calculation method was used. All 7 transitions ($\Delta M_S = \pm 1$) are assumed to be allowed in between 8 different electron spin states for this simulation.

2.5 Results and Discussion

Although it was pointed that Gd^{3+} complexes are in the weak field splitting region, these are the first direct measurements of zero field splittings for Gd^{+3} with organic ligands by EPR. The results from the simulations of EPR spectra are summarized in table 2.1. The comparisons of experimental and simulated results of Gd TTHA and Gd EDTA are shown in figure 2.2 and 2.3, respectively. As a result, the method for Gd^{3+} complexes with

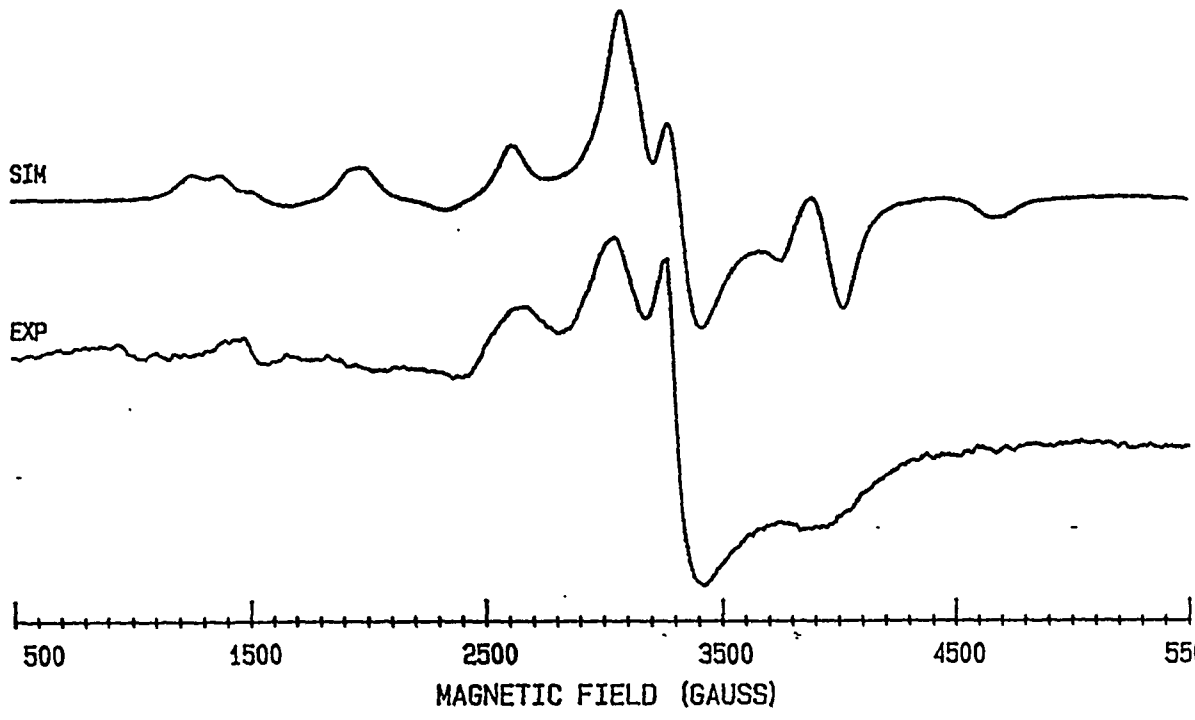

Figure 2.2 Experimental and simulated EPR spectra of Gd TTHA in water/glycerol glass at liquid nitrogen temperature. (9.30 GHz)

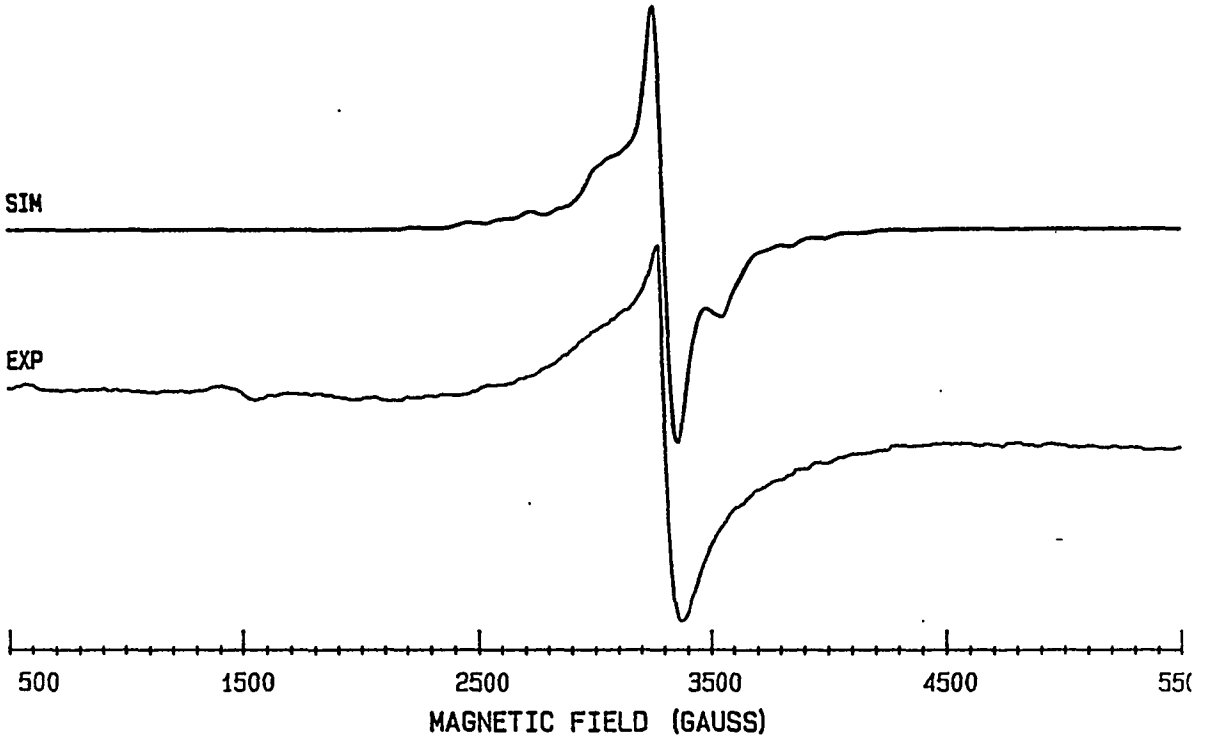

Figure 2.3 Experimental and simulated EPR spectra of Gd EDTA in water/methanol glass at liquid nitrogen temperature. (9.31GHz)

Table 2.1.

Data from EPR spectra of Gd complexes in frozen glasses at Nitrogen Temp.

	D(MHz),[cm^{-1}]	|3E/D|	g_{iso}
Gd TTHA	980 [0.033]	0.8	1.99
Gd DTPA	1500 [0.050]	0.6	2.01
Gd EDTA	400 [0.013]	0.7	1.99
Gd DOTA	< 180 [< 0.006]	-	1.99

inorganic ligands can be applied to the systems with organic ligands. For all complexes with organic ligands that we are testing, g values are isotropic, close to g = 2, and have smaller D and E values than those reported for Gd^{3+} in inorganic systems.[10), 11)] These results also suggest that the application of the Solomon-Bloembergen-Morgan equations to Gd^{3+} with chelating ligands is quite reasonable as the point of the non-distorted model assumption in those equations. Gd EDTA and Gd DOTA show very small values of D and E, Gd DOTA has almost no zero field splitting energy. The rhombic distortion (E) in Gd DOTA cannot be measured because it is negligibly small. When we consider the very symmetrical structure of the europium analog with the DOTA ligand by the X-ray crystal structure,[11)] this EPR result from Gd DOTA seems reasonable. Koenig et. al.[12)] compared zero field splitting energies of Gd DOTA and Gd DTPA from simulations of NMRD (nuclear Magnetic Resonance Dispersion). Their result showed the higher symmetry for the Gd DOTA case, it also agreed with our EPR studies.

REFERENCES

1. Solomon, I. Phys. Rev., **1955**, 99, 559

2. Bloembergen, N., J. Chem. Phys., **1957**, 27, 572,595

3. Bloembergen,N.; Morgan, L.O.,J. Chem. Phys., **1961**, 34, 842

4. Nicklin, R.C.; Johnstone, J.K.; Barnes, R.G.; Wilder, D.R., J. Chem. Phys., **1973**, 59, 1652

5. Iton, L.E.; Turkevich, J., J. Chem. Phys., **1977**, 81, 435

6. Iton, L.E.; Brodbeck, C.M.; Suib, S.L.; Stucky, G.D., J. Chem. Phys., **1983**, 79, 1185

7. Brodbeck, C.M.; Iton, L.E., J. Chem. Phys., **1985**, 83, 4285

8. Abragam, A.; Bleaney, B., Electron Paramagnetic Resonance of Transition Ions, Oxford University, London, 1970

9. Harder, R.; Chaberek, S., Inorg. Nucl. Chem., **1959**, 11, 197

10. Furniss, D.; Harris, E.A.; Hollis, D.B., J. Phys. C: Solid State Phys., **1987**, 20,L147

11. Splirlet, M-R,; Rebizant, J.; Desreux, J-F.; Loncin, M-F., Inorg. Chem., **1984**, 23, 359

12. Geraldes, C.F.G.C.; Brown, R.D.; Cacheris, W.P.; Sherry, A.D.; Spiller, M., Magn. Reson. Med., **1989**, 9, 94

CHAPTER 3

Electron Spin Echo Envelope Modulation Studies of Gd-based Contrast Agents

3.1 Background

Many factors may contribute to enhance the relaxation rate of water protons. Among them, water exchange between bulk water and the metal complexes is thought to be very important. Thus the solvation structure of the Gd complexes is of interest, because it should affect this phenomenon in great amount. According to inner sphere mechanisms for proton relaxation enhancement theory by Solomon-Bloembergen, it depends upon the term $(1/r)^6$, where r is the distance between water protons and the metal. However, not much information on the solvation structure of Gd chelate complexes is available. Here we report the result of Electron Spin Echo studies of Gd DTPA, Gd EDTA, and Gd TTHA in frozen solution. For this study we use a systematic series of Gadolinium amino poly acetic acid, Gd EDTA, Gd DTPA,and Gd TTHA with increasing the coordination number, 5,8, and 10 respectively. Those compounds are shown in figure 3.1. A reasonable apriori expectation

for number of inner sphere waters are 2 or 3 for Gd EDTA, 1 for Gd DTPA, and 0 for Gd TTHA.

3.2 Theory

3.2.1 Electron Spin Echo Experiment

The Electron Spin Echo Experiment is a pulsed technique in which electron spins are excited by microwave pulses. The first pulse induces the large rotation of the net electron spin magnetization away from equilibrium. Before the net magnetization relaxes back to equilibrium, it can be refocussed by one or more pulses. Generally one performs either a three-pulse or a two-pulse experiment. Both are described in several papers[1),2)]. In this paper, we report the result of the three-pulse experiment, thus the three-pulse experiment will be discussed here briefly. In our three-pulse experiment, the 90°-τ-90°-T-90° pulse sequence is used. Usually τ is fixed, and T, the interval between the second and third pulse is varied. The refocussed echo which occurs at a time τ after the third pulse is termed "stimulated echo". As increasing the time,T, the stimulated echo is also shifted according to T as shown in figure 3.2.

This series of echoes is called the " Electron Spin Echo Envelope". This envelope shows an oscillatory change in intensity, that is "envelope modulation". The Electron Spin Echo Envelope Modulation can be calculated by the density matrix formalism first presented by Mims,Rowan, and Hahn[3),4)]. Before introducing the appropriate equations for the deuterium system, let us look at the energy level diagram for the simplest system, for I = 1/2 and S = 1/2 in figure 3.3.

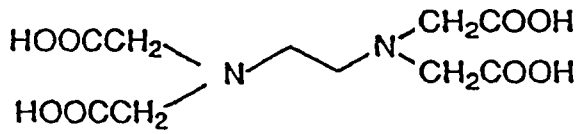

EDTA

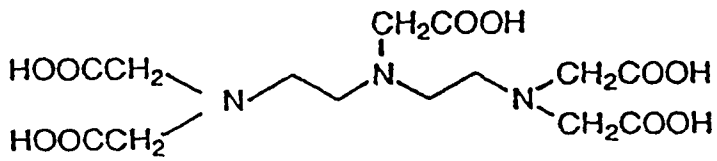

DTPA

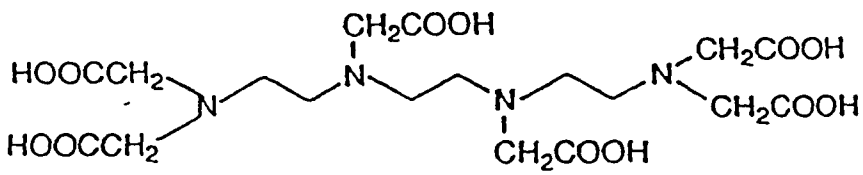

TTHA

Figure 3.1. Structures of Ligands

a) EDTA (Ethylene diamine triaceticacid)

b) DTPA (Diethylene triamine pentaaceticacid)

c) TTHA (Triethylene tetraamine hexaaceticacid)

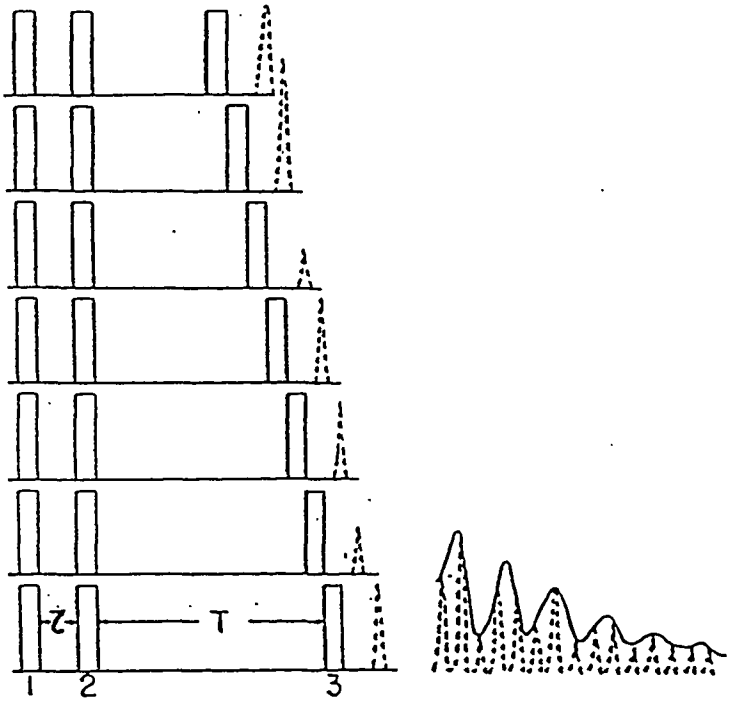

Figure 3.2. Illustration of modulation of stimulated spin echo decay envelope. The time τ between pulse 1 and pulse 2 is fixed while the time T between pulse 2 and 3 is varied. The echo appears a time τ after pulse 3.

In the high field approximation, the transitions for which $\Delta S = \pm 1$, $\Delta m = 0$ are allowed transitions and those for which $\Delta S = \pm 1$, $\Delta m = \pm 1$ are "forbidden" transitions. However the presence of hyperfine and nuclear quadrupole coupling provide that contribute the intensity to "forbidden" transition. As a result, micro wave pulses induce transitions from a common initial states to multiple final states creating coherences between the final states. These coherences result in interferences which modulate the echo envelope. The ESEEM (Electron Spin Echo Envelope Modulation) can be calculated from the transition probabilities of using density matrix formalism.

On the basis of above idea, now we consider the case of a Gd^{+3} ion surrounded by the deuterium nuclei. For Kramers doublet ion, we can employ the equation for $S = 1/2$, thus we can use the ESEEM equation for $S = 1/2$, $I = 1$, which was derived by Mims et.al.[4),5)]

The static spin Hamiltonian of the spin system can be written as

$$\mathcal{H}_o = g_e \beta_e \vec{H}_o \hat{S}_z - g_n \beta_n \vec{H}_o \hat{I}_z + \hbar a \hat{I}_z \hat{S}_z$$
$$+ g_e g_n \beta_e \beta_n / r^3 [(3\cos^2\theta - 1)\hat{I}_z + \sin\theta\cos\theta \hat{I}_x] \hat{S}_z \qquad [3.1]$$

Above four terms represent the electron Zeeman, nuclear Zeeman, Fermi contact, and dipolar interaction. where r is the distance between electron and the nucleus, and θ is the angle between H_o and the electron-nuclear axis.

For the Gd^{+3} system which has an isotropic g value and negligibly small quadrupole coupling in glassy matrix, the normalized three-pulse echo modulation for $S = 1/2$, and $I = 1$ is given in equation 3.2.[4),5)] The isotropic g value of Gd^{+3} was confirmed by our simulation

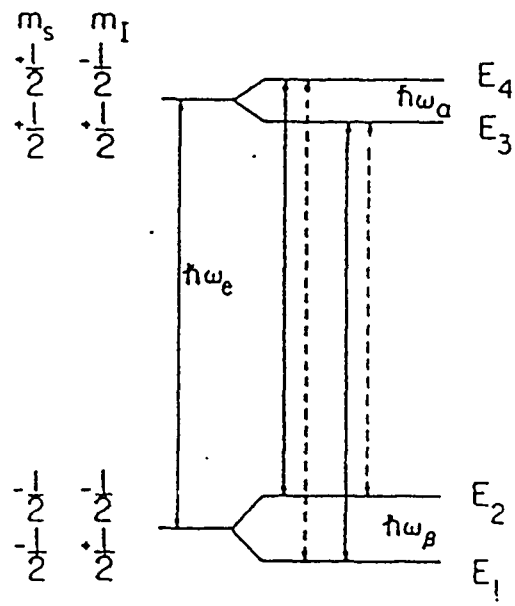

Figure 3.3. Energy level diagram of an S = 1/2, I = 1/2 spin system with positive dipolar coupling. The solid and dashed lines show allowed and forbidden transitions respectively. Simultaneous excitation of both types of transitions results modulation effects.

work of EPR spectra of Gd^{+3} in glassy matrix.[6]

$$V_{mod}(2\tau + T, l=1) = 1 - 8/3\, k[\sin^2(\omega_\alpha\tau/2)\sin^2(\omega_\beta(\tau + T)/2) + \sin^2[(\omega_\alpha(\tau + T)/2)\sin^2(\omega_\beta\tau/2)] + 8/3\, k^2[\sin^4(\omega_\alpha\tau/2)\sin^2(\omega_\beta(\tau + T)/2) + \sin^4(\omega_\alpha(\tau + T)\sin^2(\omega_\beta T/2)] \quad [3.2]$$

$$k = (\omega_I B/\omega_\alpha\omega_\beta)^2$$

$$\omega_\alpha = \{[(A/2) + \omega_I]^2 + (B/2)^2\}^{\frac{1}{2}}$$

$$\omega_\beta = \{[(A/2) - \omega_I]^2 + (B/2)^2\}^{\frac{1}{2}}$$

$$A = g_e g_n \beta_e \beta_n/\hbar r^3 (3\cos^2\theta - 1) - 2\pi a$$

$$B = 3 g_e g_n \beta_e \beta_n \cos\theta\sin\theta/\hbar r^3$$

The equation 3.2 was used for the simulations of ^{2}H-ESEEM in this work, and derived upon the following assumptions.

i) High field regime : dipolar term is less than zeeman energy.

ii) High temperature approximation.

iii) The nuclear quadrupole coupling term is small enough to be treated just as perturbation.

iv) The electron spin levels form Kramers doublets.

v) Point-dipole approximation

i) - iv) are generally accepted for X-band ^{2}H-ESE for Gd^{+3} experiment, and the validity of the point-dipole approximation depends upon the localization of electron spin density. Thus the results of this study show effective distances, which are more valid for weak long range

coupling.

The nuclear quadrupole coupling term is treated as perturbation here, and Hamiltonian for this part may be written as,

$$\mathcal{H}_Q = e^2qQ/4\,[3\hat{I}_z^2 - \hat{I}^2 - \eta(\hat{I}_x^2 - \hat{I}_y^2)\,] \qquad [3.3]$$

If we consider the asymmetry parameter η is small enough to neglect, this equation can be simplified as in the axial symmetry.

$$\mathcal{H}_Q = e^2qQ/4\,[3\hat{I}_z^2 - \hat{I}^2] = 3e^2qQ/4\,[\hat{I}_z^2 - \hat{I}^2/3] \qquad [3.4]$$

The energy level diagram including nuclear quadrupole coupling term for the deuterium system is shown in figure 3.4, Δ is in the unit of $3e^2qQ/4$.

3.2.2 Coupling with many nuclei: the Spherical Model

When a number of nuclei are coupled with the same electron spin, the total envelope modulation function is given by the product of the modulation function for each nucleus,

$$\langle V_{mod} \rangle = 1/4\pi \int_0^{2\pi}\int_0^{\pi} V_{mod}(\theta)\sin\theta d\theta d\Phi \qquad [3.5]$$

where the θ and Φ are the polar and azimuthal angles describing the orientation of the external field with the molecular coordinated system. Mims, and Kevan and as well as others[7), 8)] have shown approximating this equation by essentially reversing the order of the integration and product operations. In this approximation, they first integrate the magnetic field and then to product of the averaged modulation pattern for all nuclei. From this model it is possible to calculate an effective distance with the simpler calculation.

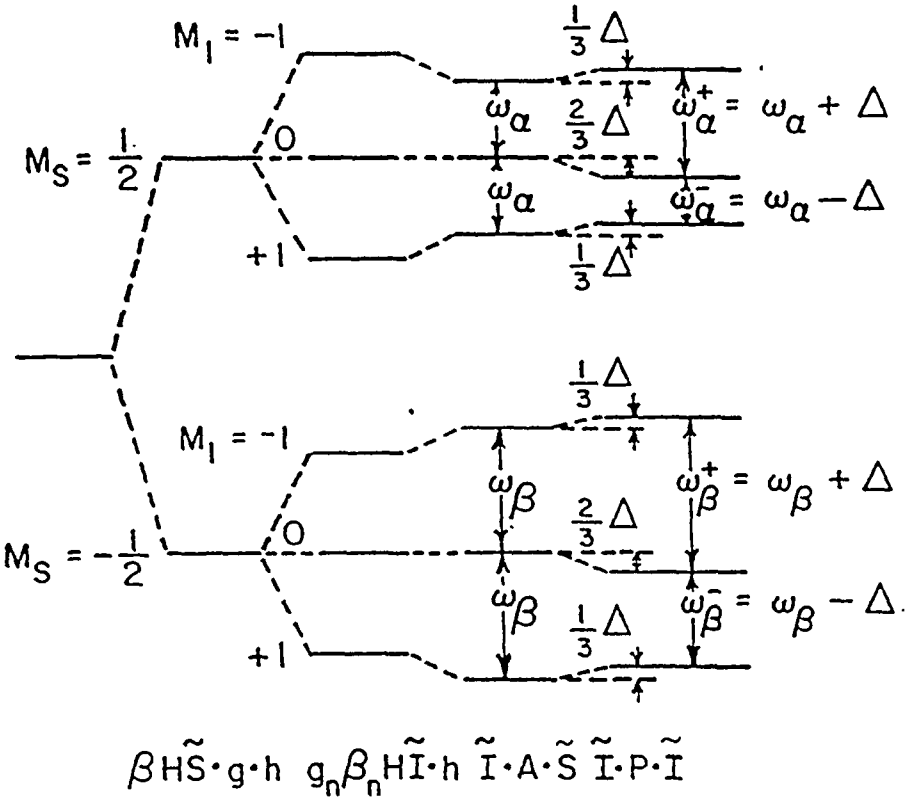

$$\beta \tilde{H}\tilde{S}\cdot g\cdot h \; g_n\beta_n \tilde{H}\tilde{I}\cdot h \; \tilde{\tilde{I}}\cdot A\cdot \tilde{\tilde{S}} \; \tilde{\tilde{I}}\cdot P\cdot \tilde{I}$$

Figure 3.4.Energy level diagram for an S = 1/2 and I = 1 spin system with positive dipolar coupling interaction.

$$<(V_{mod})^N> = 1/4\pi \int_0^{2\pi}\int_0^{\pi} \prod_{i=1}^{N} \{ V_{mod}(\theta_i)\} \sin\theta d\theta d\Phi \qquad [3.6]$$

$$\sim [<V_{mod}>]^N = [\ 1/4\pi \int_0^{2\pi}\int_0^{\pi} V_{mod}(\theta) \sin\theta d\theta d\Phi\ ]^N \qquad [3.7]$$

3.3 Experimental

Gd DTPA•Megl(meglumine), Gd EDTA•Megl, and Gd TTHA•Na_3 were synthesized at Schering Ag, Berlin, West Germany. Deuterated water and partially deuterated methanol (CH_3OD) were from Aldrich Chemical Co. Each sample was prepared in MeOD/D_2O solution, the concentration for each solution was 3mM at ~pH 7.

The Electron spin echo experiment was done at 10 K with X-band ESE spectrometer at Albert Einstein College of Medicine in New York. The computer simulations were done with a fortran program developed in our laboratory.[9]

3.4. Results and Discussion

3.4.1 General Approach

We are primarily interested in determining the solvation structure of Gd complexes. In order to distinguish the solvent hydrogens from ligand hydrogens, we use deuterated (-OD) solvents. Therefore we can examine just the structure of -OD in solvated molecules. Another

advantage of using deuterium is the deep modulation depth of deuterium.

We began our study with the ESEEM of Gd TTHA in frozen solution, because we expect it the simplest in terms of solvation structure. In aqueous solution, the stability constants for equilibrium between Gd^{+3} and TTHA ligand is 10^{23} at around pH 7.[10] Thus we believe that all the coordination sites of gadolinium are blocked by the TTHA ligand which has the potential to 10 coordination sites. Such a structure suggest that the ^{2}H-ESEEM signal of Gd TTHA is due entirely to the solvent molecules which are not directly coordinated to Gd metal, since Ga^{+3} is fully coordinated by a TTHA ligand. As a result, a simulation of the ESEEM data requiring 7 deuterons at 3.9 Å with a_{iso} = 0.10 MHz and e^2qQ = 0.37 MHz provided the best fit. The simulated and the experimental ^{2}H-ESEEM are shown in figure 3.5. In our subsequent analysis for the ESEEM of Gd EDTA and Gd DTPA, we set equal the second sphere solvent structure of Gd TTHA, Gd DTPA and Gd EDTA. This assumption allows us to exclude the second and outer sphere modulation by dividing the ESEEM of Gd EDTA and Gd DTPA by that of Gd TTHA.

The analysis of ^{2}H-ESEEM of Gd EDTA and Gd DTPA is basically same. Each ESEEM pattern of those complexes was divided by that of Gd TTHA and the remaining ESEEM was considered the signal from the deuterons in inner sphere solvent molecules. Each inner sphere ESEEM was simulated in the same way that the Gd TTHA was simulated. And finally the simulated ESEEM of Gd TTHA and inner sphere Gd EDTA were multiplied to give the whole simulated ESEEM of Gd EDTA. The simulated and experimental ESEEM of Gd EDTA are shown in figure 3.6. The summary of results is shown in table 3.1.

3.4.2 ^{2}H-ESEEM of Gd TTHA

This three pulse ^{2}H-ESEEM shows a distinct phase reversal point[11),12)] which is very

Table 3.1.

Solvent Structure of Gd Complexes (as -OD) from ^2H - ESE results at 5K

ligand	No. of ^2H	r_{eff}(Å)	a_{iso}(MHz)	e^2qQ(MHz)
EDTA	3	2.70 ± 0.05	0.30 ± 0.01	0.37 ± 0.02
	7	3.90 ± 0.05	0.10 ± 0.01	0.37 ± 0.02
DTPA	< 1	2.75 ± 0.05	0.25 ± 0.01	0.31 ± 0.02
	7	3.90 ± 0.05	0.10 ± 0.01	0.37 ± 0.02
TTHA	7	3.90 ± 0.05	0.10 ± 0.01	0.37 ± 0.02

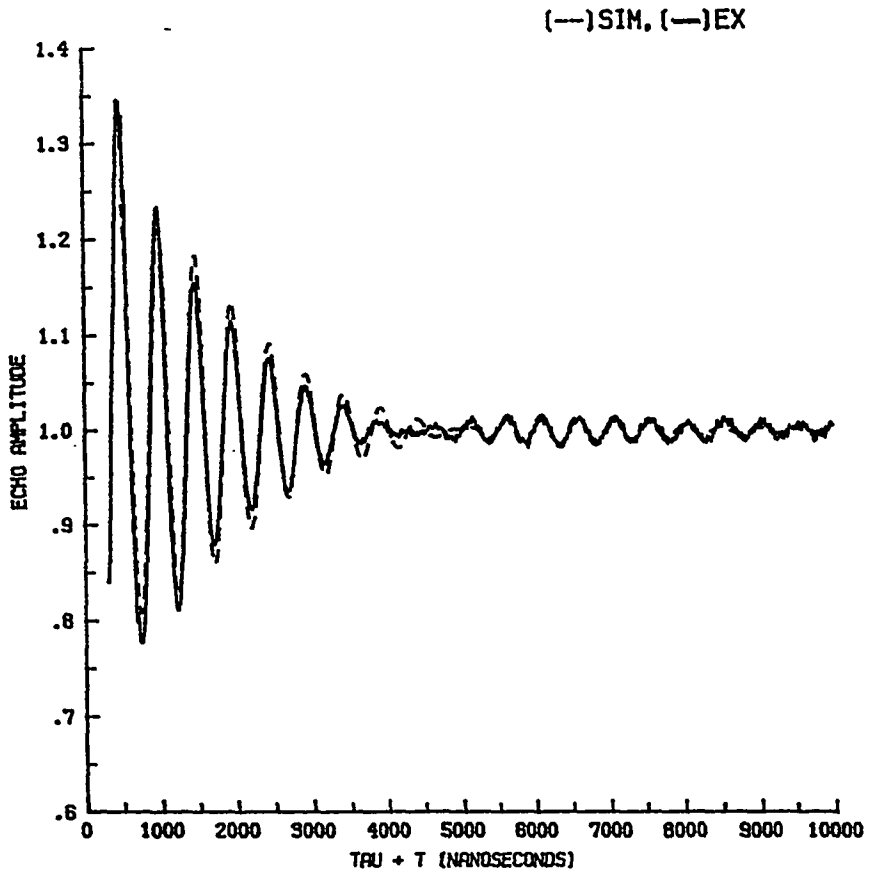

Figure 3.5. Experimental and simulated three-pulse ^{2}H-ESEEM of Gd TTHA in frozen D_2O/MeOD glass at helium temperature. $\tau = 225$ nanoseconds, H_o = 3133 G, ν = 8.7476GHz

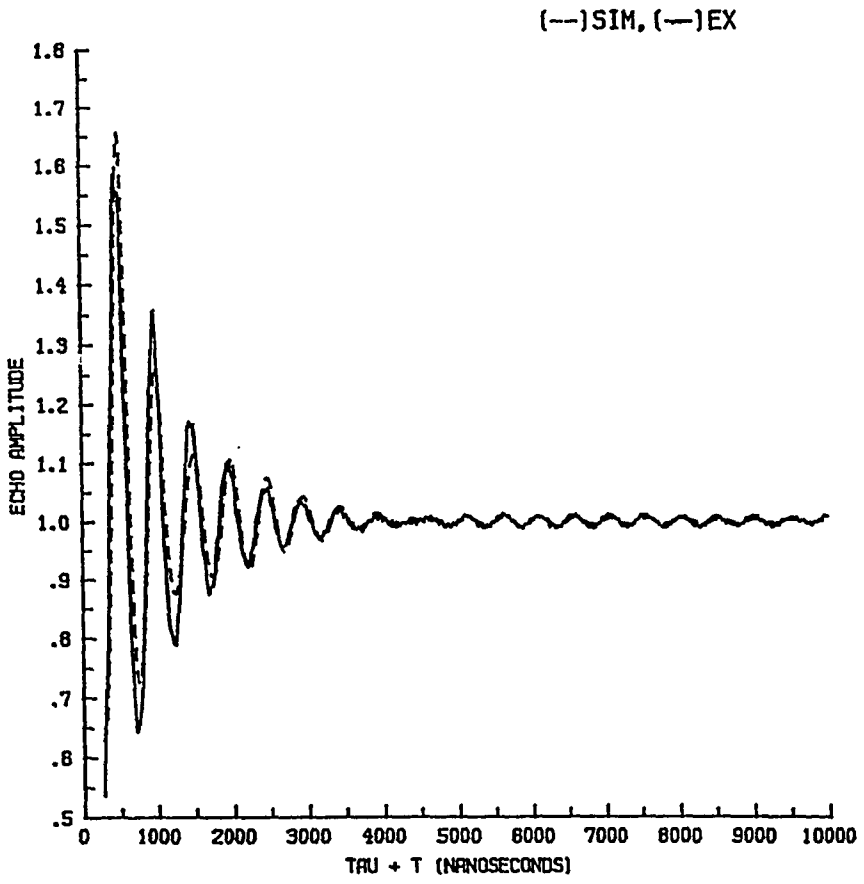

Figure 3.6. Experimental and simulated three-pulse ^{2}H-ESEEM of Gd EDTA in frozen D_2O/MeOD glass at helium temperature. τ = 187 nanoseconds, H_0 = 3133 G, ν = 8.7192 GHz

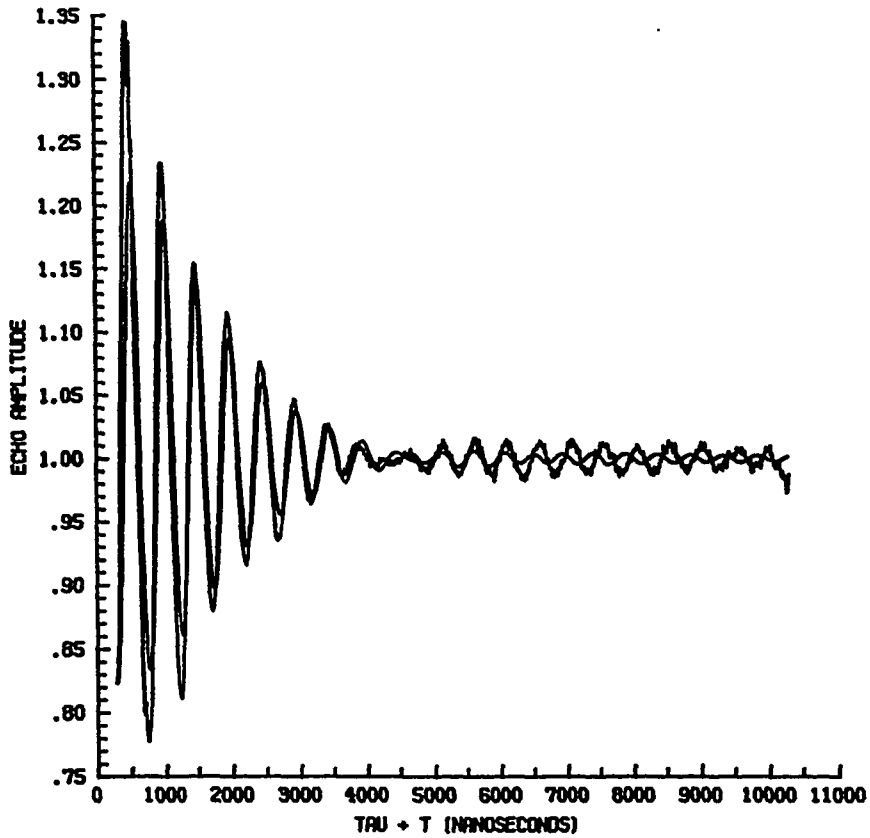

Figure 3.7. Simulated and experimental three-pulse ^{2}H-ESEEM of Gd TTHA. The experimental spectrum is exactly same as in figure 3.5, and the input parameters for the simulation are r = 3.75 Å, a_{iso} = 0.1 MHz, and e^2qQ = 0.37 MHz.

sensitive to the choice of Gd - ^{2}H distance and a_{iso}. When the simulation is done with a little smaller value of r, 3.75 Å instead of 3.9 Å, the simulated ESEEM is very off from the experimental spectrum as shown in figure 3.7. A consequence of this sensitivity of the theoretical simulations to the choice of r and a_{iso} is that the parameters chose to fit the envelope modulation from Gd TTHA are quite reliable.

For all simulations, the numbers of deuterium are constrained to be integral for easier understanding of each structure. Seven deuterons are found at 3.9 Å. Quadrupole coupling interaction is sometimes neglected for the simulations of ^{2}H-ESEEM because of small value. Waldstein et.al.[13] reported that e^2qQ and $|\eta|$ of D_2O ice were 0.215 MHz and 0.1 by NMR. The quadrupole coupling constant of deuterium in this system is 0.37 MHz, which is slightly larger than that in D_2O ice.

3.4.3 ^{2}H-ESEEM of Gd EDTA

As explained previously, second sphere solvent structure is set to be the same as that of Gd TTHA. Inner sphere solvents result shows that 3 deuterons at 2.7 Å are found. According to the X-ray crystal structure of a Gd DPTA derivative compound, the distance between water oxygen and Gd metal is 2.431 Å.[14] Also ^{1}H-ENDOR results showed that the Gd^{+3} and proton of the first coordination water distance was 2.65 -2.90 Å[15]. Our results are in good agreement with others in terms of distance. But the number of coordination sites still seems an open question. Three deuterons can never be interpreted as the three coordinated site for solvents unless we assume three methanol molecules are directly bound to Gd metal. But this is not a reasonable assumption on the basis of both steric and electrical effects. Our ESE results from Gd EDTA in frozen solution at liquid helium temperature strongly suggest two coordination sites rather than three in this system.

3.4.4 ^{2}H-ESEEM of Gd DTPA

All numbers of deuterons are constrained to be integral, however, for inner sphere solvent, it is less than 1, only 0.4 ± 0.1. That means only 20 % of Gd complexes have the one inner sphere water molecule if we assume only water molecules are directly bound to Gd metal. This is quite different from the X-ray crystal structure of Gd DTPA derivatives. In X-ray structure, Gd has definite 9 coordinate site, 8 from a DTPA ligand and 1 from a water molecule.[14] Koenig et.al.[16] also reported the fractional number of inner sphere water for some of Gd DTPA analogs by NMRD (Nuclear Magnetic Relaxation Dispersion) studies at 5°-25° C. Their results suggest that as the temperature of the system is lowed, the fraction of Gd complexes with no inner sphere water increases. Our results clearly represent a low-temperature limit for the equilibrium controlling innner sphere water occupancy in this complex, and indicate that the equilibrium constant for process Gd DTPA + H_2O ⇌ Gd DTPA • H_2O has a lower limit of q ≈ 0.2. According to these results, the coordination sites of Gd^{+3} seems flexible as in the range of 9 ± 1 in solution.

REFERENCES

1. Kevan,L.;Schwartz,R.N., " Time Domain Electron Spin Resonance";Wiley and Sons; New York, 1979; p 280

2. Hahn, E.L. Phys. Rev. **1950**, 80, 580

3. Rowan,L.G.; Hahn, L.G.; Mims,W.B. Phys. Rev. **1965**, 137, A61

4. Mims,W.B. Phys. Rev.(B) **1972**, 6, 2409, and 3543

5. Mims,W.B.; Peisach,J; Davis,J.L. J. Chem. Phys. **1977**, 66, 5536

6 Hwang,J-H; Tanner,M; Belford,R.L.; Clarkson,R.B., " Abstract of the Eight Annual Meeting of Society of Magnetic Resonance in Medicine", Amsterdam, 1989, p 797

7. Mims,W.B.; Davis,J.L. J. Chem. Phys. **1976**, 64, 4836

8. Anderson,M.W.; Kevan,L. J. Chem. Phys. **1987**, 87, 1

9. Cornelius, J., Ph.D.Thesis, University of Illinois, Urbana,Illinois (1987)

10. Lauffer,R. Chem. Rev. **1987**, 87, 901 , and references are therein.

11. Narayana, P; Kevan,L. J. Magn. Reson. **1976**, 23, 385

12. Yudanov,V.F.; Dikanov,S.A.; Tsevetkov,Y.D. J. Struct. Chem. **1976**, 17, 451

13. Wadstein,P.; Rabideau,S.; Jackson, J. J. Chem. Phys. **1964**, 41, 3407

14. Private communication with Schering AG, Berlin.

15. Yim,M.B.; Makinen, M.W. J. Magn. Reson. **1986**, 70, 89

16. Geraldes,C.F.G.C.; Sherry,A.D.; Cacheris,W.P.; Kaun,K-T.; Brown III, R.D.; Koenig, S.H.; Spiller, M. Magn. Reson. Med. **1988**, 8, 191

CHAPTER 4

O-17 NMR Studies for Water Exchange Times

4.1 Background

The proton relaxation enhancing by the paramagnetic metal effects on bulk water by the fast exchange between bulk water and the coordinated water. If the exchange rate is too fast, or too slow, the relaxation enhancing effect is less on bulk water. Thus controlling τ_M is very important for maximizing the proton relaxation enhancing. In a quantitative view, τ_M has a dual importance in relaxivity. It can contribute to the total correlation time (equation 1.15), and it modulates the efficiency of the chemical exchange of water molecules sampling the paramagnetic center (equation 1.25).

By employing the S-B-M model, normally 1-100 nano-seconds were obtained for τ_M.[1] For measuring τ_M of inner sphere water, O-17 NMR experiments were used for some previous studies by Swift and Connick[2] and modified by Merbach et. al.[3] Some τ_M values on the free metals and metal complexes with some ligands were reported by Swift and Connick methods.[4], [5] However, study of τ_M on the Gd^{3+} contrast agents is still at an early stage. We want to measure the exchange time of water in the system of Gd^{+3} and the multidentate ligands by the Merbach's modified method.

For free rotating complexes of metal ions, τ_R dominates total correlation time, τ_c. But the rotational correlation time gets longer, then the total correlation time is not dominated by τ_R for slowly tumbling molecules. In that case, τ_M can play a big role for the total correlation time. When a metal chelate is bound to proteins, the exchange time can be varied directly via hydrogen bonding interactions with the bound water or steric blocking of the water exchange pathway to the bulk solvent. In this chapter, Gd^{3+} complexes with proteins will not be discussed, only unbound Gd^{3+} contrast agents will be studied.

4.2 O-17 Experiments by the Merbach Method

4.2.1 Theoretical background

All theoretical background of this experiment is based on the S-B-M model, which was already described in chapter 1. The equations for relaxation times are as follows, where 'a' stands for the site of bulk water, and 'M' stands for the metal site.

$$1/\tau_{aM} >> |1/T_{2a}-1/T_{2M}| \qquad [4.1]$$

$$1/\tau_{aM} >> |1/T_{1a}-1/T_{1M}| \qquad [4.2]$$

$$1/\tau_{aM} >> \Delta\omega_{aM} \qquad [4.3]$$

$$Gd\ DTPA{\bullet}(H_2O) \xrightarrow{k_{Gd}} Gd\ DTPA + (H_2O) \qquad [4.4]$$

If the exchange rate is shorter than the separation of those two peaks, the peaks cannot be resolved. Only averaged one peak is observed at the averaged frequency,

$$\omega_{obs} = \omega_a f_a + \omega_M f_M \qquad [4.5]$$

with relaxation times,

$$1/T_2 = f_a/T_{2a} + f_M/T_{2M} + f_a f_M \tau_M \Delta\omega_{aM}^2 \qquad [4.6]$$

$$1/T_1 = f_a/T_{1a} + f_M/T_{1M} \qquad [4.7]$$

where $\Delta\omega_{aM} = \omega_{obs} - \omega_{H2O}$, the shift between bound and bulk resonances in the absence of exchange, and $1/\tau_{aM} = 1/\tau_a + 1/\tau_M$, where τ_a is the life time of the O-17 nuclei in the a site before exchange to the M(metal) site. The f_a, f_M values express the statistical probability of being in site a or M sites available divided by the sum of the a and M sites,

$$f_M = n[m]/55.6 \qquad [4.8]$$

where [m] is the molal concentration of the paramagnetic compound added.

In the gadolinium systems studied, the isotropic shift $\Delta\omega_{aM}$ is small enough that the exchange broadening condition is sufficient to ensure that the third term in equation is deleted. Then equation is reduced,

$$1/T_2 = f_a/T_{2a} + f_M/T_{2M}. \qquad [4.9]$$

Assuming that there is no significant outer sphere relaxation of the bulk water, T_{1a} is about equal to T_{2a}.

$$1/T_2 - 1/T_1 = f_a(1/T_{2a} - 1/T_{1a}) + f_b(1/T_{2M} - 1/T_{1M}). \qquad [4.10]$$

$$\approx f_b(1/T_{2M} - 1/T_{1M}) \qquad [4.11]$$

Generally five mechanisms are listed for explaining T_{1M} and T_{2M}.[4] However, the quadrupolar relaxation as well as relaxation by spin rotation , T_1 and T_2 and these terms will be canceled in equation 4.11.

By analogy with studies of C-13 relaxation, the relaxation due to chemical shift anisotropy is probably a few hundreds seconds and this will never make significant effect on the relaxation times observed in this study.

The remaining two mechanisms we have to consider are,

i) dipole-dipole coupling between the magnetic moment of the unpaired electrons

and the O-17 nuclei,

ii) and the Fermi contact coupling between two.

4.2.1.1 Fermi Contact Interaction

By the S-B-M equations, the contact terms are as follows,

$$1/T_1^s = (S(S+1)/3)(A/h)^2[2\tau_{e2}^2/(1 + \omega_s^2\tau_{e2}^2)] \quad [4.12]$$

$$1/T_2^s = (S(S+1)/3)(A/h)^2[\tau_{e1} + \tau_{e2}/(1 + \omega_s^2\tau_{e2}^2)], \quad [4.13]$$

where the superscript 's' denotes scalar contact terms.

If $\omega_s^2\tau^2 >> 1$, fast motional at high field, $1/T_1^s$ term will be very small.

4.2.1.2. Dipole-dipole Interaction

The important point of the O-17 NMR study is that there is a chemical bond between the O-17 and the Gd^{3+} metal, while there is no chemical bond between the water proton and the Gd^{3+} metal. It was reported that the contribution of dipole-dipole to the quantity $(1/T_2 - 1/T_1)$ in equation 4.11 was only 0.8%.[3] Thus the dipolar interaction can be neglected in these O-17 NMR experiments.

At the high field and fast motional region, the following equations are derived.

$$\omega_s^2\tau^2 >> 1,\ 1/T_2^s >> 1/T_1^s \quad [4.14]$$

$$1/T_2 - 1/T_1 = f_M(1/T_{2M} - 1/T_{1M}) = f_M(1/T_{2M}^s - 1/T_{1M}^s)$$

$$= f_M/T_{2M}^s = f_M(S(S + 1)/3)(A/h)^2(\tau_{e1} + \tau_{e2}/(1 + \omega_s^2\tau_{e2}^2))$$

$$\approx f_M(S(S + 1)/3)(A/h)^2\tau_{e1} \quad [4.15]$$

$$1/\tau_{e1} = 1/\tau_M + 1/T_{1e} \quad [4.16]$$

Merbach et.al. assume that the isotropic shift of Gd(III) is majorly due to the contact interaction,

$$\Delta\omega/\omega = A_{iso}f_M(\gamma_S/\gamma_I)[S(S+1)/3kT] \qquad [4.17]$$

where ω is the frequency of instrument $\Delta\omega$ is the measured isotropic shift by the O-17 NMR experiments.

As in chapter 2, no hyperfine or distortion of EPR lines due to coupling with the magnetic isotopes of gadolinium (^{155}Gd:14.73 % and ^{157}Gd:15.68% both with I = 3/2) could be observed. Therefore we concluded that any contribution to line broadening due to this hyperfine interaction is negligible. In solution EPR, many T_{1e} from 7 electronic spin states cannot be separable. The data were treated using McLachlan theory of averaged relaxation theory in chapter 1. We assumed that the D and E values are not functions of temperature and the correlation time τ_v exhibits Arrhenius behavior, i.e.

$$\tau_v = \tau_v^{o}\exp(E_a/kT). \qquad [4.18]$$

And Eyring kinetic theory shows,

$$1/\tau_M = k_{Gd} = (kT/h)\exp(-\Delta H^{\ddagger}/RT + \Delta S^{\ddagger}/R). \qquad [4.19]$$

Finally, the optimal $k_{Gd} = 1/\tau_M$ values were solved based on equations 4.15-4.19 by the use of a multiple regression.

4.2.3 T_1 and T_2 measurement by O-17 NMR

Regular 5 mm NMR tubes were used for T1-IR experiments, and coaxial tubes were used for measuring isotropic shifts. All NMR parameters were measured at 40.678 MHz by using GN 300 NB spectrometer at the University of Illinois at Urbana-Champaign. And $\pi/2$ pulse length was ~ 30 μsec. Transverse relaxation times, T_2, were obtained by Lorentzian

fitting the spectrum and each full-width at half-maximum were measured from a fitting program of the spectrometer. Longitudinal relaxation times, T_1, were obtained by the inversion recovery method, the height of each peak were measured by a ruler and height were curve fit to a three parameter function,

$$M_z(\tau) = M_0 [1-(1-k)\exp(-\tau/T_1)] \qquad [4.20]$$

as the equation was discussed by Levy and Peat.[7] The temperature was measured by using the variable temperature unit of the GN 300NB spectrometer.

4.3 Results and Discussion

4.3.1 Gd^{3+} Aqua Complex and Gd EDTA

In order to test our method, the experiment on the free Gd^{3+} was repeated and compared our results with the reported ones.[3] As in table 4.1, our values are very close to reported ones. By the same method, data on Gd EDTA were also analyzed. The results on those compounds are summarized in table 4.4.

4.3.2 Gd DTPA

This experiment on Gd DTPA gave an unexpected results. As we have seen the equations, 4.10 and 4.19. The plot of ln $1/f_M \cdot (1/T_2 - 1/T_1)$ versus (1/Temp.) is approximately linear according to equations 4.15 - 4.19. However, this plot for Gd DTPA is very off from a linearity. This means that Gd DTPA complex shows some different behavior from Gd EDTA and Gd^{3+} aqua compounds. One can expect that it might be due to the inconsistency of the q number as the temperature is varied. Overall, Merbach's Method seems to be good enough

for Gd EDTA and the Gd^{3+} aqua complex, but it might be too crude to deal more complicated system like Gd DTPA. A new model might be needed for study of Gd^{3+} contrast agents, such as Gd DTPA.

Table 4.1

O-17 Relaxation times of Gd^{3+} aqua ion at V.T.

T(K^o)	T_1(msec)	T_2(msec)
10	3.51	0.978
20	4.86	1.23
30	6.68	1.53
40	7.29	1.84
50	9.09	2.16

Table 4.2

O-17 Relaxation Times of Gd EDTA at V.T.

Temp(^{o}C)	T_1(msec)	T_2(msec)
10	4.46	1.24
20	5.67	1.68
30	7.03	2.11
40	8.75	2.69
50	10.23	3.11

Table 4.3

O-17 Relaxation Times of Gd DTPA at V.T.

Temp(°C)	T_1(msec)	T_2(msec)
10	1.92	1.25
20	2.50	1.28
30	3.28	1.34
40	4.10	1.60
50	5.04	1.97
60	6.74	2.61

Table 4.4

Water exchange data of free Gd^{+3} and Gd EDTA from O-17 NMR

	Free Gd^{3+}		Gd EDTA
	Merbach's data[3), a)]	this work[b)]	
	8.314, 12.20 (MHz)	40.38 MHz	40.38 MHz[b)]
$k_{Gd} \times 10^{-8}$ sec^{-1}	11.0, 7.9, 10.6	9.64	4.56
$\Delta H^{\ddagger}$ KJ/mol	11.96, 14.96, 11.99	12.36	15.94
$\Delta S^{\ddagger}$ J/K mol	-31.75, -27.58, -31.91	-31.3	-25.4

a) At 25°C.

b) At 21.6°C.

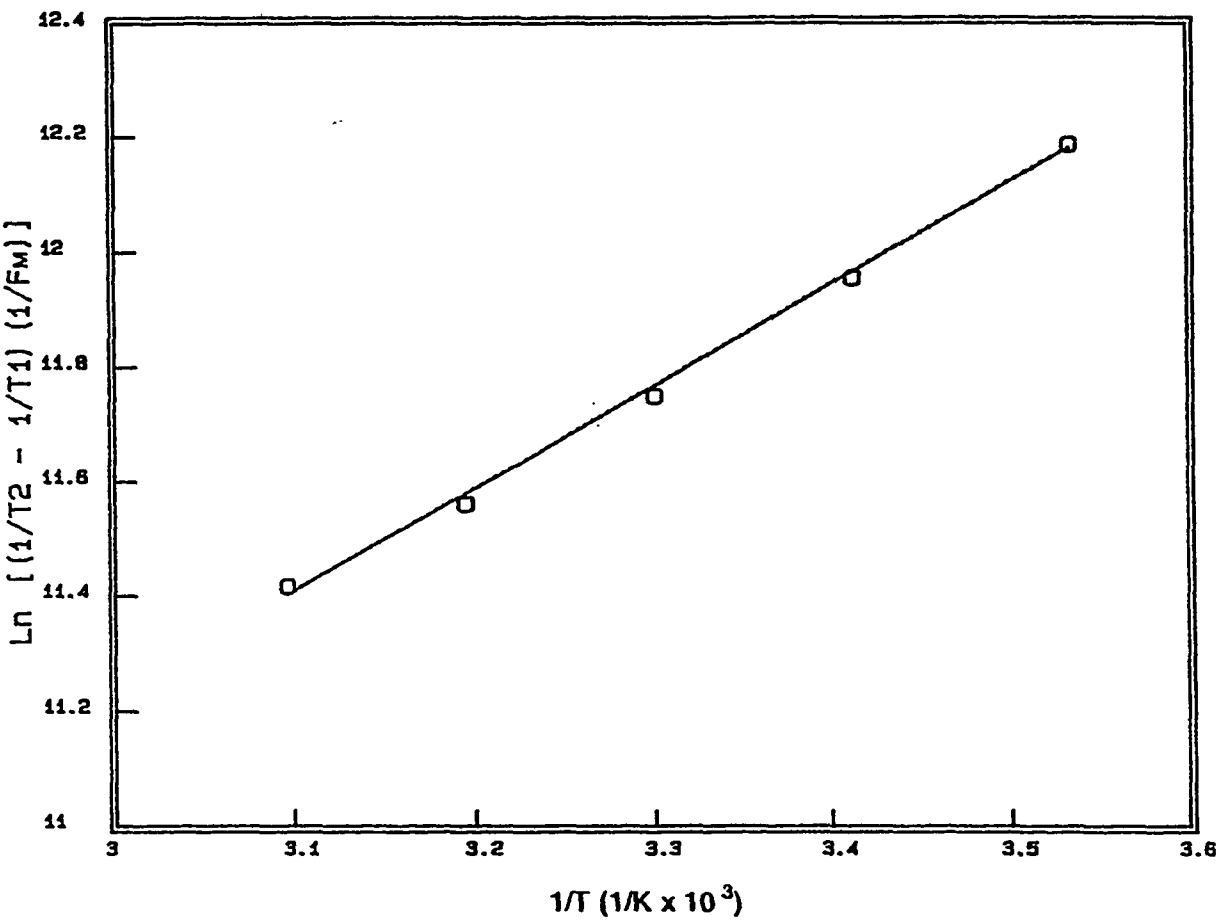

Figure 4.1. The Plot of $1/f_M(1/T_2 - 1/T_1)$ versus (1/Temp.) on Gd Aqua Complexes

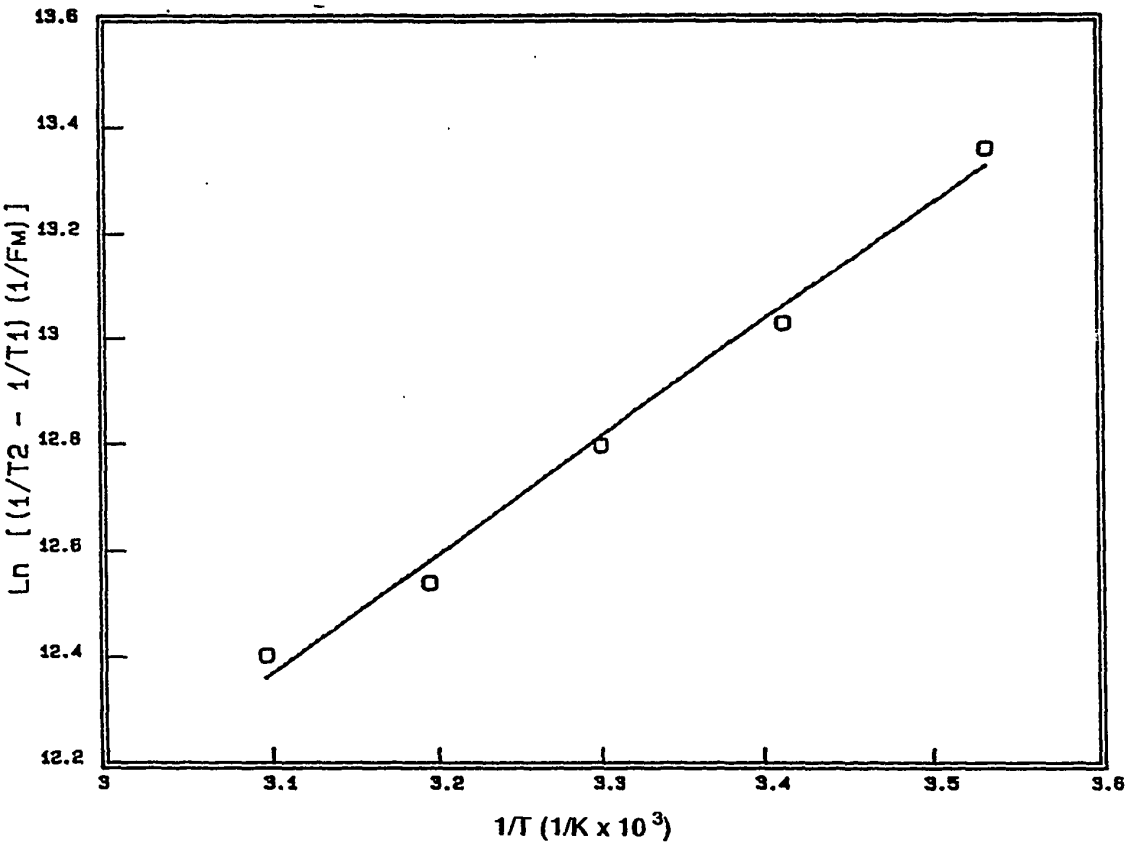

Figure 4.2. The Plot of $1/f_M(1/T_2-1/T_1)$ versus (1/Temp.) on Gd EDTA

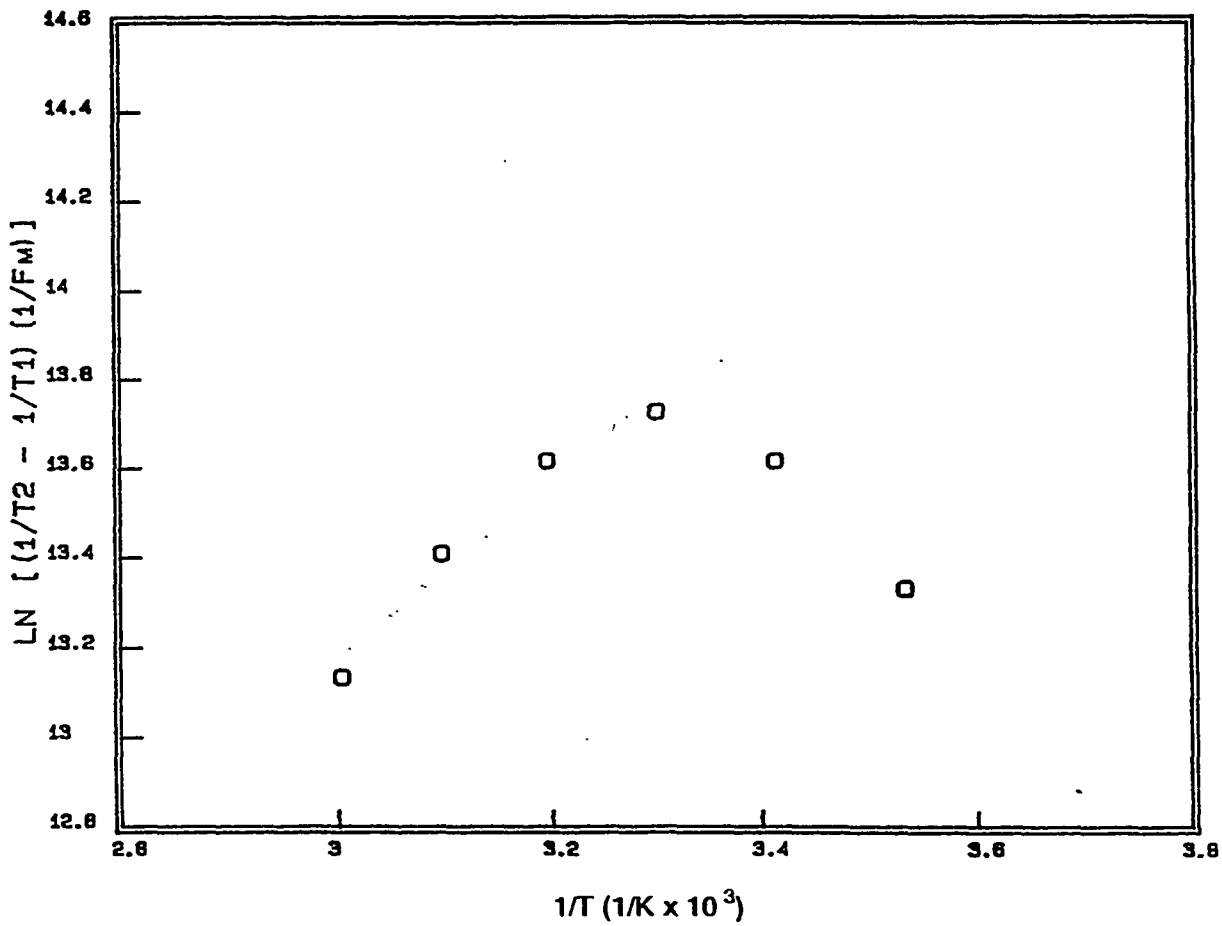

Figure 4.3 The plot of $1/f_M(1/T_2-1/T_1)$ versus (1/Temp.) on Gd DTPA

REFERENCES

1. Lauffer, R. B. Chem. Rev., **1987**, 87, 901

2. Swift, T.J.; Connick, R.E.; J. Chem. Phys., **1962**, 37, 307

3. Southwood-Jones, R.V.; Earl, W.L.; Newman,K.E.; Merbach, A.E., J. Chem. Phys., **1980**, 73, 5909

4. Zetter, M.S.; Grant, M. W.; Wood, E.J.; Hunt, J.P., Inorg. Chem., **1972**, 11, 2701

5. Ostrich, I.J.; Liu, G.; Dodgen,H.W.; Hunt, J.P., Inorg. Chem., **1980**, 19, 619

6. Farrar, T.C.; Becker, E.D., "Fourier Transform NMR", Academic Press, New York, 1971

7. Levy, G.C.; Peat, I.R., J. Magn. Reson., **1975**, 18, 500

CHAPTER 5

Nuclear Magnetic Relaxation Dispersion Experiment and Analysis of NMRD Profiles

5.1 Background

Nuclear magnetic relaxation dispersion, NMRD, is the set of data representing the dependence of nuclear longitudinal relaxation rates($1/T_1$) on the strength of the magnetic field. The measurements of longitudinal and transverse relaxation rates can be made practically with any regular NMR spectrometer. The problem with this experiment is that each spectrometer can do only one magnetic field. If we want to do several different fields, there is the inconvenience of changing the sample from one machine to another and different signal to noise ratio. With the field cycling relaxometer, the bulk of the relaxation rates can be measured at from a very low field to a high field(up to 50 MHz for the relaxometer at the University of Illinois). This field cycling relaxometer was originated by Redfield,[1] and the advantage of it is that the spins may be polarized at a high field strength, which ultimately provide a large signal, switched to a field of desired measurement, and then switched to a

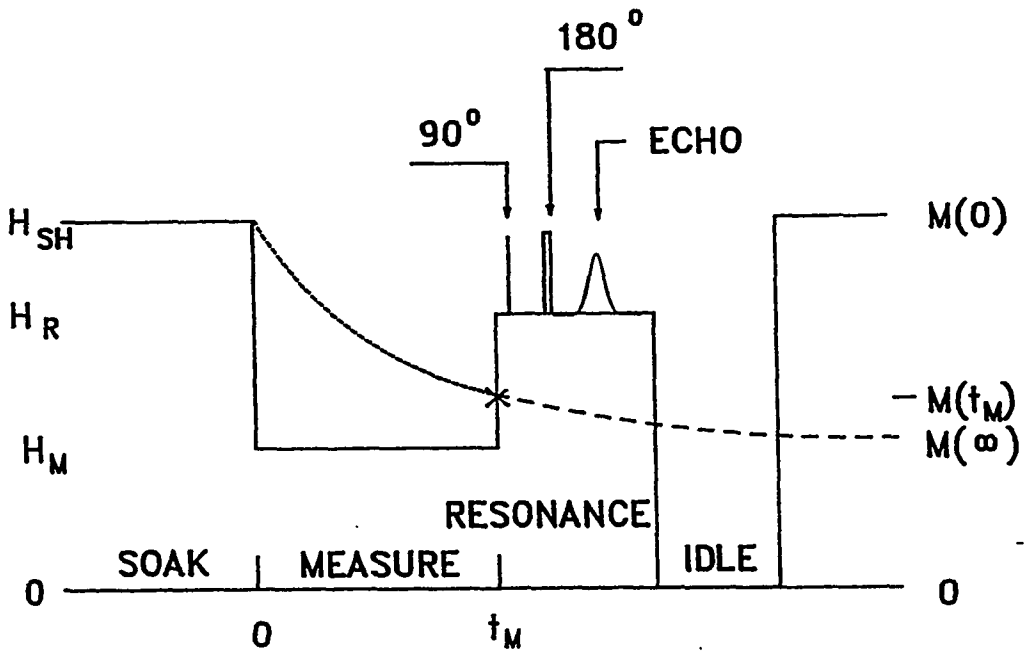

Figure 5.1. Field Cycling Relaxometer

field that is convenient for observing the remaining magnetization. Thus the data may be obtained over a wide range of field strength at practically constant signal-to-noise ratio. Figure 5.1 [2] shows the field cycling of the relaxometer. There is considerable value in taking dispersion of the nuclear relaxation rate, compared to one measurement at one field, because it may provide dynamic and chemical information that cannot be obtained from the data at a single magnetic field. The dispersion plot represents a graph of spectral power density as a function of the Larmor frequency and thus provides a direct map of the Fourier transform of the autocorrelation function for the process during nuclear spin relaxation in the sample. Therefore the dispersion is directly related to the Solomon-Bloembergen-Morgan equations (equations 1.15 -1.18) described in chapter 1. The detailed description of SBM equations will not be repeated in this chapter. In addition, the equations 1.22 -1.25 are used for analyzing the NMRD data.

5.2 Experimental

NMRD measurements were made with the field-cycling relaxometer at Biomedical Magnetic Resonance Laboratory at the University of Illinois at Urbana, that switches magnetic field strength as shown in figure 5.1. That system employs copper-wound solenoid bathed in liquid nitrogen to handle the heat dissipation. The probe is a single saddle coil coaxial line forming a component of the resonant probe circuit. In a typical experiment the spins are first brought to a proton resonance frequency at the soak magnetic field and polarized there for $5T_1$ (soak rate). A series of measurement times, t_M are used for each relaxation time

determination, and the data are fit with a non-linear least-square procedure. the statistical errors are typically about 1 %. The pyrex test tube of 10 mm diameter are used for the sample cell and stopped with a rubber stopper. The temperature is controlled by a flow of Freon that is thermostated in an external temperature control unit.

All Gd Complexes were prepared by Schering-AG, Berlin, Germany. Each solution was prepared in 1 millimolar solution at around pH 7.

5.3 Experimetal Results

The results of relaxation rates of gadolinum complexes in water are summerized in tables 5.1-5.11.

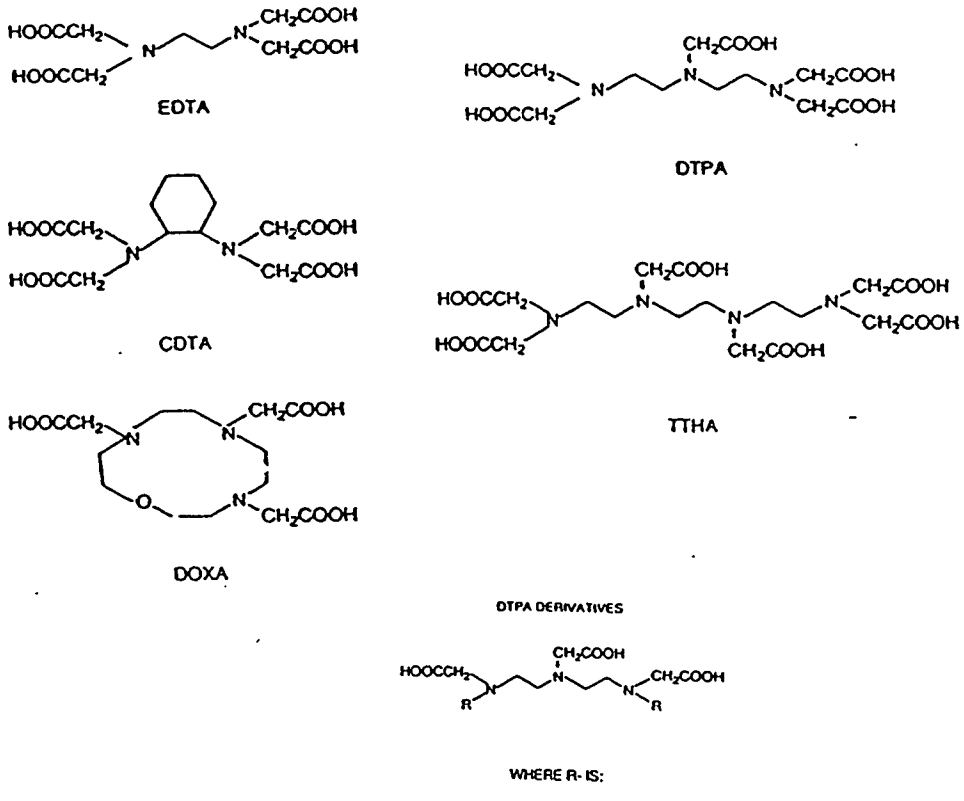

Figure 5.2 Structures of Ligands Studied

Table 5.1

Relaxation Rates of Gd(TTHA)•Na_3 in Water

M.W. = 714.66 q = 0 T = 21.6°C pH = 7

Proton Larmor Frequency (MHz)	Relaxation Rate(mM•sec)$^{-1}$
0.01	4.155
0.02	4.101
0.05	4.137
0.1	4.121
0.2	4.125
0.5	4.084
0.75	4.060
1	4.038
2	3.913
3	3.812
5	3.542
7.5	3.249
10	3.026
15	2.707
20	2.550
30	2.347
40	2.278
50	2.275

Table 5.2

Relaxation Rates of Gd(DTPA)•$MegI_2$ in Water

M.W. = 938 q = 1 T = 21.6°C pH = 7

Proton Larmor Frequency(MHz)	Relaxation Rate $(mM \cdot sec)^{-1}$
0.01	8.381
0.02	8.390
0.05	8.426
0.1	8.380
0.2	8.400
0.5	8.304
0.75	8.295
1	8.208
2	8.049
3	7.850
5	7.351
7.5	6.808
10	6.373
15	5.759
20	5.418
30	5.149
40	5.063
50	5.005

Table 5.3

Relaxaton Rates of Gd DOTA•Na in Water

M.W. = 580.628 q = 1 T = 21.6°C pH = 7

Proton Larmor Frequency(MHz)	Relaxation Rate(mM•sec)$^{-1}$
0.01	10.345
0.02	10.383
0.05	10.314
0.1	10.322
0.2	10.325
0.5	10.133
0.75	9.865
1	9.799
2	8.880
3	8.119
5	6.755
7.5	5.745
10	5.166
15	4.379
20	4.379
30	4.113
40	4.015
50	3.919

Table 5.4

Relaxation Rates of Gd DOXA in Water

M.W. = 501.59 q = 1 or 2 T = 21.7°C pH = 7

Proton Larmor Frequency(MHz)	Relaxation Rate(mM•sec)$^{-1}$
0.01	10.838
0.02	10.803
0.05	10.776
0.1	10.900
0.2	10.754
0.5	10.790
0.75	10.731
1	10.613
2	10.323
3	9.858
5	9.014
7.5	8.142
10	7.317
15	6.572
20	6.158
30	5.931
40	5.796
50	5.826

Table 5.5

Relaxation Rates of Gd EDTA•MegI in Water

M.W. = 641.69 q = 2 or 3 T = 21.6°C pH = 7

Proton Larmor Frequency(MHz)	Relaxation Rate $(mM \cdot sec)^{-1}$
0.01	16.794
0.02	16.628
0.05	16.576
0.1	16.578
0.2	16.825
0.5	16.580
0.75	16.469
1	16.347
2	15.610
3	14.366
5	12.659
7.5	11.147
10	10.042
15	8.840
20	8.281
30	7.731
40	7.590
50	7.579

Table 5.6

Relaxaion Rates of Gd CDTA•Megl in Water

M.W. = 695.78 q = 1 T = 21.6°C pH = 7

Proton Larmor Frequency(MHz)	Relaxation Rate(mM•sec)$^{-1}$
0.01	14.225
0.02	14.071
0.05	14.061
0.1	14.210
0.2	14.082
0.5	14.041
0.75	13.986
1	13.777
2	13.331
3	12.836
5	11.369
7.5	10.468
10	9.597
15	8.732
20	8.304
30	7.713
40	7.571
50	7.616

Table 5.7

Relaxation Rates of Gd (DTPA-polymer) [ZK 119985] in Water

M.W. = ~40,000 q = 1 T = 21.6°C pH = 7

Proton Larmor Frequency (MHz)	Relaxation Rate $(mM \cdot sec)^{-1}$
0.01	10.504
0.02	10.492
0.05	10.492
0.1	10.550
0.2	10.439
0.5	10.317
0.75	10.113
1	9.977
2	9.496
3	9.333
5	9.287
7.5	9.464
10	9.925
15	10.336
20	10.623
30	10.619
40	10.578
50	10.476

Table 5.8

Relaxation Rates of Gd (DTPA-polymer) in Water

M.W. = ~50,000 q = 1 T = 21.6°C pH = 7

Proton Larmor Frequency (MHz)	Relaxation Rate $(mM \cdot sec)^{-1}$
0.01	11.755
0.02	11.732
0.05	11.756
0.1	11.690
0.2	11.684
0.5	11.502
0.75	11.265
1	11.209
2	10.694
3	10.472
5	10.324
7.5	10.761
10	11.282
15	11.835
20	12.314
30	12.577
40	12.643
50	12.728

Table 5.9

Relaxation Rates of Gd DTPA Deriv 1, [Z.K.118407] in Water

M.W. = 767.90 q = 1 T = 21.6°C pH = 7

Proton Larmor Frequency(MHz)	Relaxation Rate $(mM \cdot sec)^{-1}$
0.01	6.055
0.02	6.057
0.05	6.092
0.1	6.074
0.2	6.053
0.5	5.972
0.75	5.975
1	5.903
2	5.764
3	5.594
5	5.323
7.5	5.052
10	4.830
15	4.489
20	4.399
30	4.237
40	4.191
50	4.187

Table 5.10

Relaxation Rates of Gd DTPA deriv. 2. [ZK 118421] in Water

M.W. = 767.99 q = 1 T = 21.6°C pH = 7

Proton Larmor Frequency(MHz)	Relaxation Rate $(mM \cdot sec)^{-1}$
0.01	5.967
0.02	5.98
0.05	5.953
0.1	5.960
0.2	5.937
0.5	5.916
0.75	5.845
1	5.787
2	5.663
3	5.516
5	5.278
7.5	5.002
10	4.740
15	4.488
20	4.293
30	4.156
40	4.127
50	4.117

Table 5.11

Relaxation Rates of Gd DTPA Deriv. 3. [ZK 130774] in Water

M.W. = 713.84 q = 1 T = 21.6°C pH = 7

Proton Larmor Frequency (MHz)	Relaxation Rate $(mM \cdot sec)^{-1}$
0.01	6.093
0.02	6.107
0.05	6.106
0.1	6.112
0.2	6.120
0.5	6.043
0.75	6.010
1	5.965
2	5.806
3	5.636
5	5.298
7.5	5.037
10	4.815
15	4.477
20	4.351
30	4.174
40	4.172
50	4.117

5.4 Simulations of NMRD Profiles

5.4.1 General Approach

All the simulations were done by a computer program based on the Solomon-Bloembergen equations [equations 1.15 -1.18]. Each NMRD curve was fitted to non-linear least square program written in BASIC. Input parameters are τ_R = rotational correlation time, τ_v = zero field modulation correlation time, τ_M = exchange correlation time, τ_{SO} = zero field correlation time which can be converted to zero field splitting energy, and q= the numbers of inner sphere water. Isotropic metal-nuclei hyperfine coupling constant, a_{iso}, and r= the distance between water proton and the central metal, are input as fixed parameters. For this simulation called NFQ, we set the relaxivity from the outer sphere water equal for all Gd^{3+} complexes studied. The relaxivity of Gd TTHA was set to be a standard for the outer sphere relaxivity of the other Gd complexes. For other complexes which have both inner and outer sphere waters, the outer sphere contribution was removed by subtraction of the relaxivity of Gd TTHA. Then only the inner sphere contribution was simulated by this simulation program. Finally the sum of the relaxivity of Gd TTHA and the simulated relaxivity of the inner sphere water give the total relaxivity of a certain Gd^{3+} complex. Many simulation works on paramagnetic contrast agents have been done by Koenig, but there is a difference in his program and ours for treating electron relaxation times.[3] The theoretical comparison was reviewed in chapter 1. Thus the simulations in this chapter are based on more conventional way of McLachlan's relaxation theory.[4]

The simulation results are summarized in Table 5.12. It cannot be ruled out that these NMRD simulations include some ambiguity because this program has seven

independent parameters to fit a simple dispersion curve. To make these simulations more valid, some values are taken from the separate results in previous chapters.

Normally q values are assumed from apriori expectation values. For instance, the simulations of Gd DOTA and Gd DTPA were started with the q values close to 1.0. For those of Gd CDTA and Gd EDTA, the apriori q value is 3. That of Gd DOXA was chosen between 1 and 2, because the DOXA is a hepatadentate ligand. Simulations for Gd^{3+} with several derivatives of DTPA were cumbersome, because we do not have enough information on the structures of them. The preliminary simulations were done based on the assumptions that those unsymmetrical structures would give longer rotational correlation time and those hydrophilic substituents might cause the longer exchange correlation time than Gd DTPA.

As τ_{SO} values are directly related to zero field splitting, those were always referred to the EPR spectra of corresponding compounds. The zero field modulation correlation time τ_v is assumed to be related to the vibrating and wedging motions of waters bound to the central metal. For all the complexes, we expected little difference in water solution, and those values were constricted in the range of 1 - tens of pico second unit.

The rotational correlation time τ_R is assumed to be dependent upon the molecular weight of the compound. For small compounds, with molecular weights smaller than 1,000, the simulation was done in the range that τ_R is less than 100 psec.

As τ_M of some complexes were measured by the O-17 NMR experiment, those values in the NMRD simulation were fixed at the nano second unit or close to it.

TABLE 5.12

Results from the NMRD Simulations of Gd Complexes at 21.6°C

	M.W.	q	τ_R (psec)	r(Å)	τ_M (nsec)	τ_{SO}^* (sec^2)	τ_v (psec)	q[5]
Dd EDTA•MegI	641.69	2	70	3.0	4.9	5.4×10^{-20}	35	2.5
Gd CDTA•MegI	695.78	2	70	3.0	5.4	2.2×10^{-20}	25	2.5
Gd DOXA	501.50	1.24	75	3.0	9.0	3.5×10^{-20}	37	-
Gd DTPA•MegI	742.79	0.92	81	3.0	2.3	2.4×10^{-20}	36	1.2
Gd DOTA•Na	580.63	0.82	72	3.1	9.0	1×10^{-19}	4.6	1.2
Gd(DTPA-trimer)	2,320	0.5	235	2.9	4.0	4.0×10^{-20}	47	-
Gd(DTPA-polymer)	~50,000	0.42	640	2.8	1.0	5.2×10^{-20}	49	

* This τ_{SO} is different from Koenig's τ_{SO} in tems of the definition and the units.

5.4.2 Gd EDTA and Gd CDTA (q > 2)

According to the structures of Gd EDTA and GD CDTA, q values of those complexes are supposed to be 2 or 3. The results from the simulation of NMRD curves gave only 2 for both complexes. It was found that 2.5 water molecules are bound to both complexes by the luminescence experiments of the europium analogs. From the simulation of both complexes, all parameters except τ_{SO} are found to be extremely similar to each other. Because of the slightly different structures of these complexes, the different zero field splittings are expected. The τ_{SO} value of Gd EDTA is found to be greater than that of Gd CDTA. That results in the longer electronic relaxation time for Gd EDTA and higher relaxivity at lower field as shown in figure 5.3. This agrees with our EPR studies of both complexes. Zero field splitting values of Gd CDTA is found to greater than that of Gd EDTA by EPR studies.

5.4.3 Gd DOXA (1 < q < 2)

The structure of Gd DOXA is in figure 5.2. It is a heptadentate ligand modified from DOTA. It is assumed that the q values is greater than that of Gd DOTA, but smaller than that of Gd EDTA. The result from the NMRD simulation gave 1.24 for Gd DOXA, which is quite reasonable. All the other values are quite close to other complexes. It suggests that there is no dramatic change in the structure of Gd DOXA except in the increase of the q value. The simulated and the experimental NMRD curves are in figure 5.4.

5.4.4 Gd DOTA and Gd DTPA (q ~ 1)

These two complexes are most popular contrast agents because they meet the basic requirements as contrast agents, high relaxivity and safety. As both have one inner sphere water molecule, they are often compared each other.[6] In NMRD curves, Gd DOTA shows higher relaxivity at lower field as in figure 5.5. According to our simulations of both complexes, this difference is mainly due to the longer electronic relaxation time of Gd DOTA according to our results. Gd DOTA is smaller and symmetrical complex than Gd DTPA. It again agrees with our EPR results. For both complexes, q values are found to be less than one. They are smaller than one found by the luminescence experiments. For some reason, the q values from our NMRD simulations are consistently smaller than one from the luminescence experiments of europium analogs.

5.5 Comparisons of Zero Field Splitting Constants from NMRD and EPR Simulations

The values of averaged zero field constants of some Gd^{3+} complexes from NMRD and EPR simulation are summarized in table 5.13. For some complexes, the values from those two techniques do not agree with each other. The NMRD simulations of using the values from EPR simulations were also attemted. However, the other values, for example, τ_R went too high to be a reasonable value by forcing the zero field splitting value kept constant. According to present results, the simulations that allow the zero field splitting value to vary to fit the NMRD profiles seem to give more reasonable data.

5.6 Comparisons of Results on Gd EDTA by Various Magnetic Resonance Methods

As a result, the values from several different experiments on Gd EDTA show

agreement with one another. Table 5.14 shows the comparisons of the values from the various magnetic resonance methods.

Table 5.13

Comparisons of Zero Field Splitting from NMRD and EPR Simulations

Complex	$(2/3D^2 + 2E^2)^{1/2}$ [cm^{-1}]		
	NMRD(this work)[a]	NMRD(Koenig's results)[b]	EPR[c]
Gd DOTA	0.015	<0.046	<0.01
Gd EDTA	0.022		0.013
Gd DTPA	0.032	0.046	0.043
Gd DOXA	0.026		0.021

a) At 21.6°C.

b) In Koenig's paper[6], he reported quantitative values of τ_{SO} and τ_v at 25°C for Gd DTPA, but gave a just qualitative explanation for Gd DOTA, that has longer eletronic relaxation times than Gd DTPA.

c) At liquid nitrogen temperature.

Table 5.14

Data on Gd EDTA from Several Methods

Measurement	r(Å)	q	$(2/3D^2 + 2E^2)^{1/2}$ (cm^{-1})	T_{1e} (nsec)	T_{1e} (nsec)	τ_M (nsec)	τ_R (psec)
EPR[a]			0.013				
ESE[b]	2.6	2					
O-17 NMR[c]		2				3.7	
NMRD[c]	3.0	2	0.022	0.22	0.20	4.9	57

a) At nitrogen temperature.

b) At helium temperature.

c) At 21.6°C

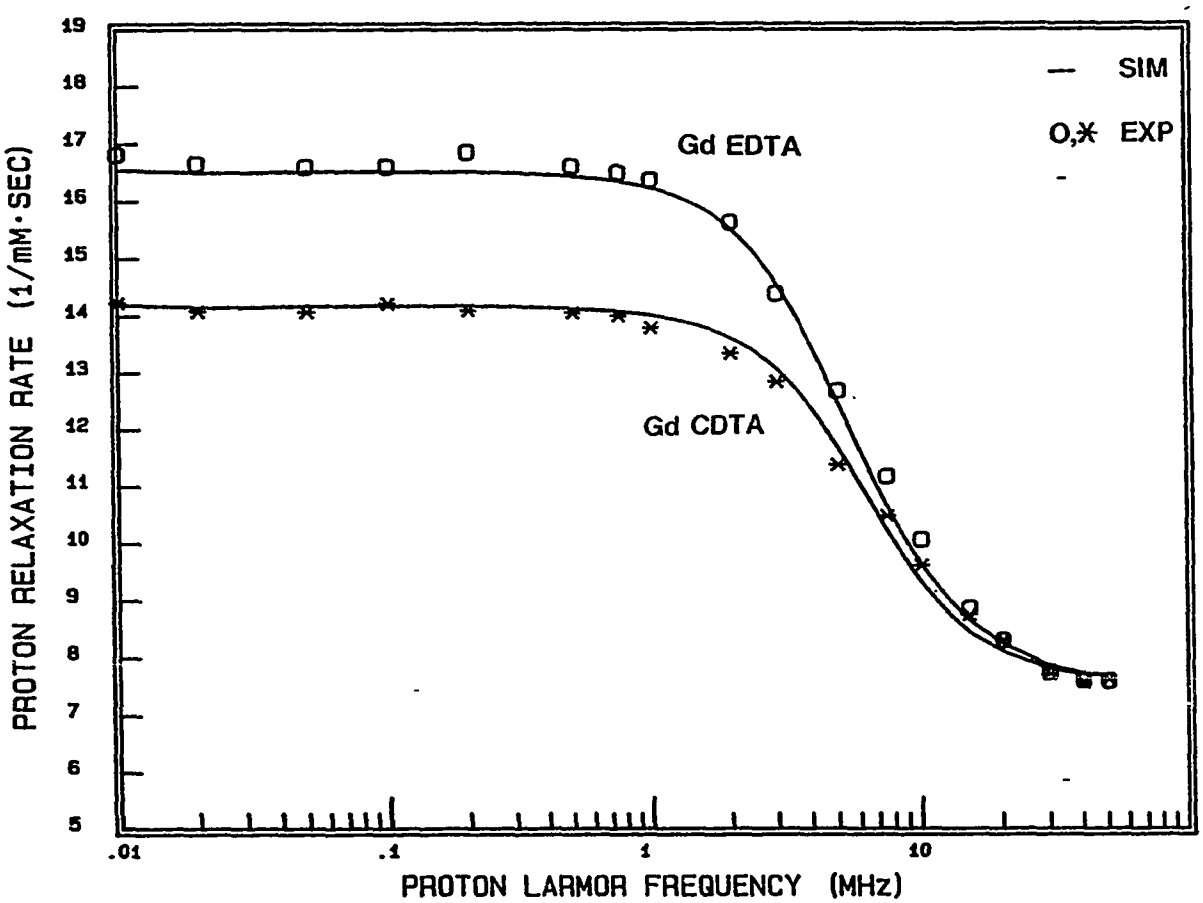

Figure 5.3. Experimental and Simulated NMRD Profiles of Gd EDTA and Gd CDTA

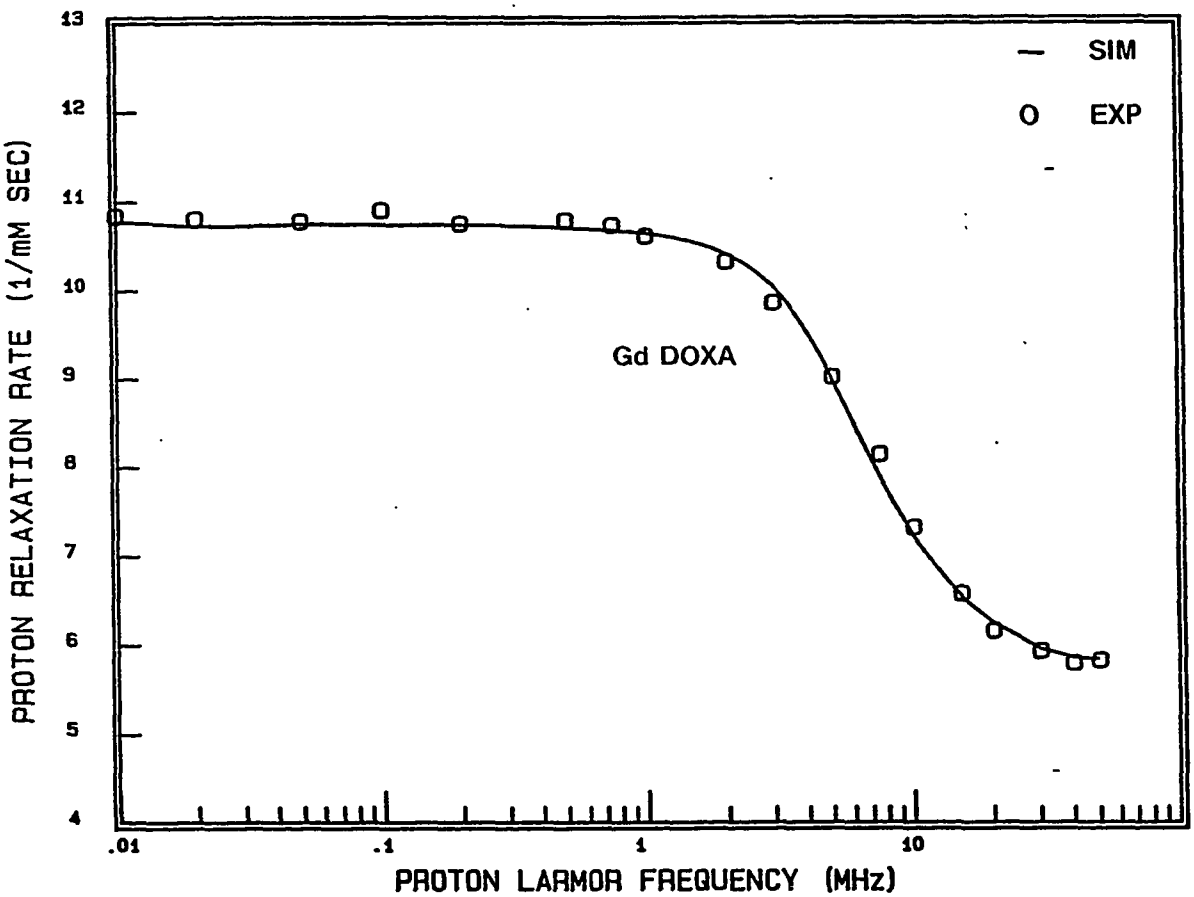

Figure 5.4. Experimental and Simulated NMRD Profile of Gd DOXA

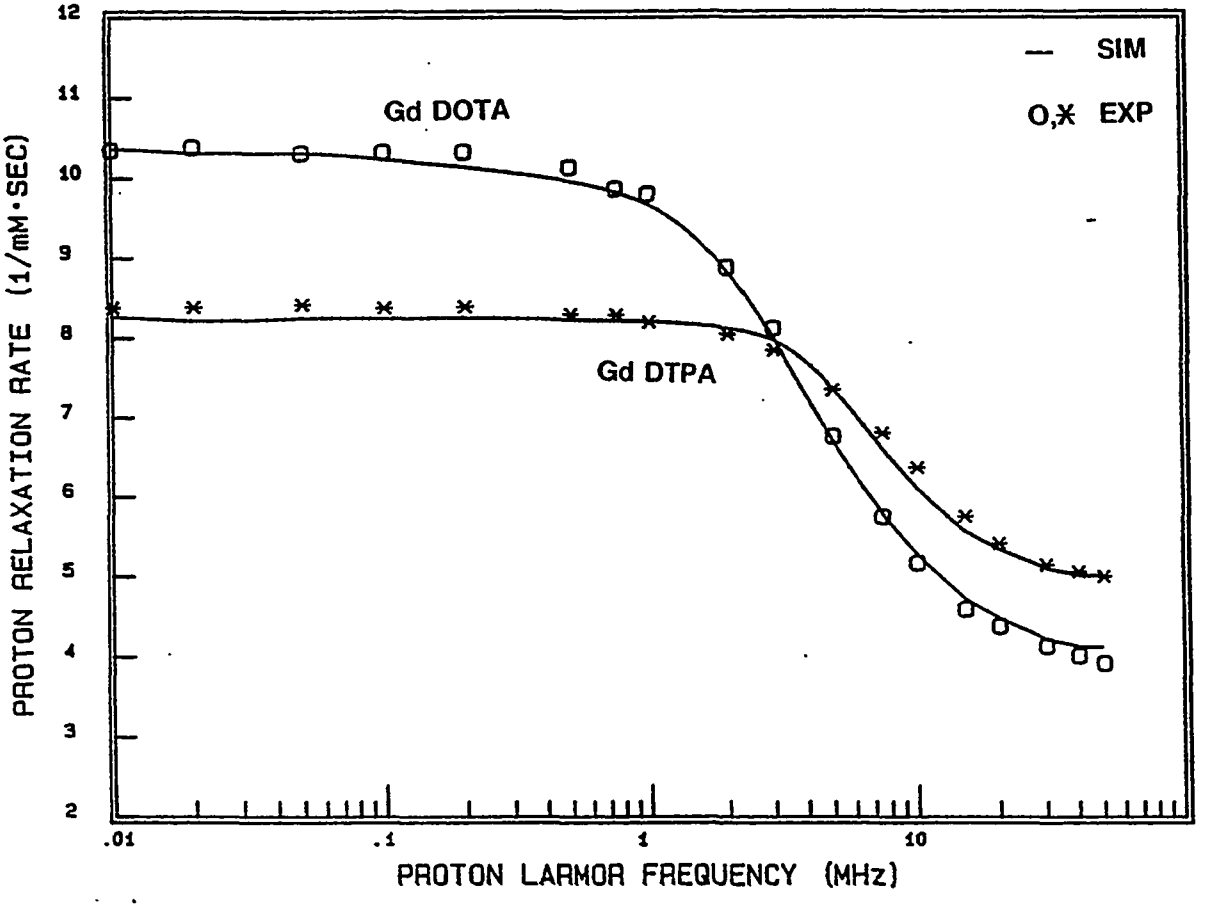

Figure 5.5 Experimental and Simulated NMRD Profiles of Gd DOTA and Gd DTPA

REFERENCES

1. Redfield,A.G.; Fite,W.; Bleich,H.E., Rev. Sci. Instr., **1968**, 39, 710

2. The Manual of the Field Cycling Relaxometer of University of Illinois at Urbana-Champaign

3. Koenig, S.H.; Epstein,M., J. Chem. Phys., **1975**, 63, 2279

4. McLachlan,A.D., Proc. R. Soc.,**1964**, A280, 271

5. Bryden, C.C.; Reilley,C.N., Anal. Chem., **1982**, 54, 610

6. Geraldes, C.F.G.C.; Brown,R.D.; Cacheris,W.P.; Koenig, S.H.; Sherry, A.D.; spiller,M., Magn. Reson. Med., **1989**, 9, 94

CHAPTER 6

Investigation of A New Class of Gd-based Contrast Agents

6.1 Background

For the diagnostic purpose, Gd DTPA shows excellent results in brain and renal systems. In general, hydrophilic complexes such as Gd DTPA cannot cross blood vessel, but cross where the Blood-Brain Barrier breaks. That causes the great contrast enhancing in tumor area in brain imaging. And unfortunately those hydrophilic complexes do not have enough bind to plasma proteins, the hepatobiliary system does not show much uptake of those kind of contrast agents. As soon as Gd DTPA is injected intravenously, it is rapidly cleared by renal excretion. Another disadvantage of Gd DTPA is that has high osmolar pressure. Gd DTPA is an anionic complex with the counter ion, sodium or meglumine ion, that shows ~ 1,900 mOsm/kg.[1)] This charged complex usually show higher osmolar pressure than that of blood plasma(300 mOsm/kg)[2)]. That results in discomfort or pain to patients. To improve comfort, the osmolar pressure should be down to the range of human plasma. One of the easiest ways to solve this problem is to make a non-anionic complex. Studies of several Gd complexes with non-ionic ligands will de discussed in this chapter. As Gd DTPA

does not make good contrast in hepatobiliary system, in vivo targeting contrast agents are developing by two different ways. One is by attaching Gd^{3+} complexes to plasma proteins or to lipids covalently,[3), 4), 5)] and the other is by attaching Gd^{3+} complexes to macromolecule non-covalently.[6), 7)] However, we have to keep in mind that the retention time of macromolecule in a human body is longer, then the possibility of free Gd^{3+} being liberated from the system is greater. That may induce the undesirable long-term toxicity.

The development of new type of Gd-based contrast agents has been made by some pharmaceutical companies and academic research groups. One of new approaches have been studied by us. By the collaboration work with Schering-AG, Berlin, studies of new complexes will be discussed in this chapter.

6.2 Experimental

NMRD and other physical experiments were basically the same as described in previous chapters. The measurements in human plasma and human serum albumin were added when it is necessary. All Gd DOTA and Gd DO3A derivative complexes were synthesized by Schering AG, Berlin. The structures studied are in figure 6.1.

Human Plasma

Human plasma from a healthy donor was obtained from the Champaign County Blood Bank and plasma was centrifuged to remove residual white and red blood cells, and kept at 0-5°C. Experiments in human plasma were done within 48 hours after the blood was drawn from the donor.

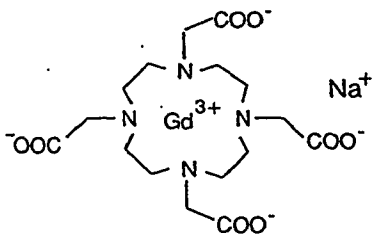

Gd DOTA

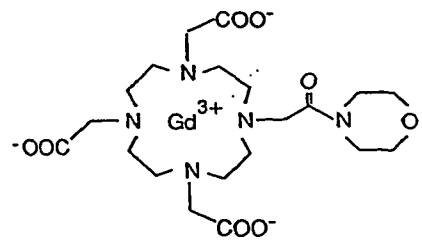

Gd DO3A Deriv.1

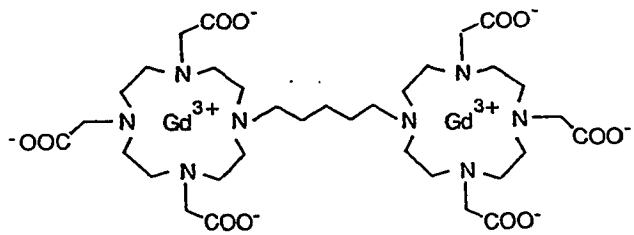

Gd DOTA Dimer

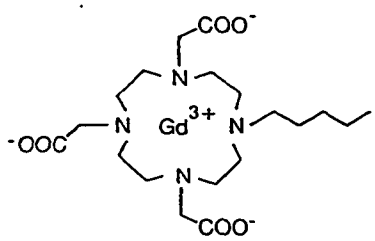

Gd DOPTA

1,4,7,10-tetraazacyclodecane-N-petanyl-N',N'',N'''-triacetic acid

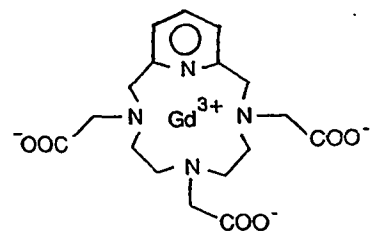

Gd (pyridine-DO3A)

Figure 6.1 Structures of Complexes Studied

Human Serum Albumin

Sterile human serum albumin in solution was purchased from Sigma Co. (St. Louis, USA). Distilled water was added to purchased human serum albumin solution to prepare the desired concentration of albumin.

6.3 Results and Discussion

The relaxation measurements in water and human plasma are summarized in Table 6.1-6.14. For some Gd^{3+} complexes, the relaxivity measurements in human albumin solution were also done.

6.3.1. Gd DOTA and Gd complexes with hydrophilic DO3A derivatives

As the DTPA and the DOTA ligands are very hydrophilic, it was already reported that Gd^{3+} complexes with those ligands do not show any interaction with plasma proteins.[8] The work for the modifications of these ligands is being done in order to reduce osmolarity and to make some in vivo targeting contrast agents. The Gd^{3+} complexes with the modified DO3A derivatives were tested here. The results of NMRD experiments are in table 6.1-6.5 and figure 6.2-6.3. As expected, the hydrophilic ligands, DO3A derivative 1 and 2 did not show any big difference in both water and human plasma in relaxivities. If we remove the diamagnetic contribution by subtracting it, NMRD curves in both water and human plasma are essentially the same. As a result, the Gd^{3+} complexes with the hydrophilic ligands do not bind to the plasma proteins in a quantity that is detectible through NMRD experiments.

6.3.2 Gd DOTA Dimer and Gd DOPTA

The NMRD curves of both complexes in human plasma show a small local maximum at high field in figure 6.4. For Gd DOTA dimer, it is quite clear, but it is not strong enough to determine for Gd DOPTA case. The other difference between the two compounds is the relaxivity change in water and human plasma. For the Gd DOTA dimer, the relaxivities in human plasma are definitely enhanced. That can be easily explained by the enhancement due to binding to macromolecules. However, the relaxivities of Gd DOPTA in human plasma are about the same or less than those of in water. That can be difficult to explain as a binding behavior. In order to clarify these experiments, the NMRD measurements in human albumin solution were carried out. These complexes have long aliphatic chains, and it is assumed that there must be interaction between these complexes and the fatty acid carrier, albumin. In figures 6.5 and tables 6.6-6.11, the results of the NMRD experiments are shown. In purified albumin solutions, both complexes show a definite local maximum at high field. It is almost clear that these complexes have strong interaction with albumin non-covalently. But it is still not known why Gd DOPTA shows slightly different results in purified human albumin and in human plasma.

6.3.3 Gd (pyridine-DO3A)

The pyridine-DO3A is one of the modified DO3A ligands, which form non-ionic complexes with Gd^{3+}. The pyridine ring replaces the one of carboxylic acid groups. Compared to Gd DOPTA and Gd DOTA dimer, it is assumed to be less lipophilic. Figure 6.6 and table 6.12-13. show the results of NMRD experiments of Gd (pyridine-DO3A). This does not show a clear maximum in human plasma and in purified albumin, but a very weak hump. This may be a sign of binding behavior to plasma proteins. It is not clear enough to

determine this only by NMRD experiments. More experiments are needed for correct characterization the behavior of this compound.

6.3.4 NMRD Simulations

The results from NMRD simulations are summerized in table 6.18.

Table 6.1

Relaxation Rates of Gd DOTA in Human Plasma

M.W. = 580.63 q = 1 T = 21.6°C pH = 7.4

Proton Larmor Frequency(MHz)	Relaxation Rate$(mM \cdot sec)^{-1}$
0.01	15.469
0.02	15.387
0.05	15.100
0.1	15.010
0.2	14.940
0.5	14.324
0.75	13.897
1	13.487
2	11.833
3	10.786
5	8.940
7.5	7.780
10	7.090
15	6.387
20	5.990
30	5.700
40	5.575
50	5.032

Table 6.2

Relaxation Rates of Gd DO3A deriv. 2.[ZK 136821] in Water

M.W. = 604.71 q = 1 T = 21.6°C pH = 7

Proton Larmor Frequency(MHz)	Relaxation Rate(mM•sec)
0.01	7.786
0.02	7.871
0.05	7.790
0.1	7.738
0.2	7.726
0.5	7.721
0.75	7.621
1	7.513
2	7.229
3	6.843
5	6.161
7.5	5.441
10	5.086
15	4.538
20	4.336
30	4.281
40	4.126
50	4.010

Table 6.3

Relaxation Rates of Gd DO3A deriv.2.[ZK136821] in Human Plasma

M.W. = 604.21 q = 1 or 2 T = 21.6 pH = 7

Proton Larmor Frequency(MHz)	Relaxation Rate$(mM \cdot sec)^{-1}$
0.01	12.036
0.02	11.860
0.05	11.789
0.1	11.636
0.2	11.364
0.5	11.131
0.75	10.804
1	10.660
2	9.755
3	9.300
5	8.280
7.5	7.500
10	7.010
15	6.775
20	6.520
30	6.330
40	6.236
50	6.048

Table 6.4

Relaxation Rates of Gd DO3A Deriv. 1.[ZK 135886] in Water

M.W. = 627.75 q = 1 or 2 T = 21.6°C pH = 7.4

Proton Larmor Frequency(MHz)	Relaxation Rate(mM•sec)$^{-1}$
0.01	8.300
0.02	8.36
0.05	8.31
0.1	8.4
0.2	8.32
0.5	8.21
0.75	8.16
1	8.04
2	7.54
3	6.91
5	6.051
7.5	5.245
10	4.78
15	4.4
20	4.165
30	3.97
40	3.85
50	3.86

Table 6.5

Relaxation Rates of Gd DO3A deriv.1.[ZK 135886] in Human Plasma

M.W. = 627.75 q = 1 or 2 T = 21.6°C pH = 7.4

Proton Larmor Frequency(MHz)	Relaxation Rate(mM•sec)$^{-1}$
0.01	12.39
0.02	12.499
0.05	12.365
0.1	12.152
0.2	12.022
0.5	11.443
0.75	11.197
1	11.049
2	10.031
3	9.107
5	7.96
7.5	6.88
10	6.38
15	6
20	5.696
30	5.49
40	5.32
50	4.94

Table 6.6

Relaxation Rates of Gd DOPTA [ZK 135335] in Water

M.W. = 570.73 q = 1 T = 21.6°C pH = 7

Proton Larmor Frequency(MHz)	Relaxation Rate(mM•sec)$^{-1}$
0.01	9.802
0.02	9.846
0.05	9.833
0.1	9.709
0.2	9.887
0.5	9.714
0.75	9.648
1	9.589
2	9.161
3	8.717
5	8.212
7.5	7.745
10	7.377
15	6.892
20	6.643
30	6.440
40	6.474
50	6.361

Table 6.7

Relaxation Rates of GdDOPTA [ZK 135335] in Human Plasma

M.W. = 570.73 q = 1,2 21.6°C pH = 7.4

Proton Larmor Frequency(MHz)	Relaxation Rate(mM•sec)$^{-1}$
0.01	10.437
0.02	10.608
0.05	10.258
0.1	10.081
0.2	9.682
0.5	9.069
0.75	8.651
1	7.741
2	7.694
3	7.261
5	6.902
7.5	6.777
10	6.761
15	6.914
20	6.785
30	6.571
40	6.055
50	5.287

Table 6.8

Relaxation Rates of Gd DOPTA [ZK 135335] in 4.5% Human Albumin

M.W. = 570.73 q = 1 T = 21.6°C pH = 7.4

Proton Larmor Frequency(MHz)	Relaxation Rate(mM•sec)$^{-1}$
0..01	12.393
0.02	12.496
0.05	12.392
0.1	12.212
0.2	11.850
0.5	11.361
0.75	10.925
1	10.546
2	9.906
3	9.463
4	9.255
7.5	9.410
10	9.709
15	10.083
20	10.176
30	9.854
40	9.234
50	7.952

Table 6.9

Relaxation Rates of Gd DOTA Dimer in Water

M.W. = 1075.41 q = 1 T = 21.6°C pH = 7

Proton Larmor Frequency(MHz)	Relaxation Rate $(mM \cdot sec)^{-1}$
0.01	12.654
0.02	12.661
0.05	12.682
0.1	12.592
0.2	12.529
0.5	12.492
0.75	12.521
1	12.517
2	11.963
3	11.337
5	10.682
7.5	10.048
10	9.636
15	9.517
20	9.366
30	9.225
40	9.241
50	9.283

Table 6.10

Relaxation Rates of Gd DOTA dimer in Human Plasma

M.W. = 1075.41 q = 1 T = 21.6°C pH = 7.4

Proton Larmor Frequency(MHz)	Relaxation Rate$(mM \cdot sec)^{-1}$
0.01	21.9
0.02	21.84
0.05	21.61
0.1	21.635
0.2	21.225
0.5	20.312
0.75	19.876
1	19.23
2	17.966
3	17.273
5	16.218
7.5	15.901
10	15.967
15	16.387
20	16.458
30	16.167
40	15.559
50	15.164

Table 6.11

Relaxation Rates of Gd DOTA dimer(0.5mM) in 4.5% albumin

M.W. = 1075.41 q = 1 T = 21.6°C pH = 7

Proton Larmor Frequency (MHz)	Relaxation Rate(0.5 mM•sec)$^{-1}$
0.01	12.217
0.02	12.127
0.05	11.764
0.1	11.745
0.2	11.604
0.5	11.082
0.75	10.527
1	10.489
2	9.880
3	9.423
5	8.860
7.5	8.859
10,	9.054
15	9.292
20	9.594
30	9.336
40	9.098
50	7.784

Table 6.12

Relaxation Rates of Gd pyridine-DO3A [ZK 132407] in Human Plasma

M.W. = 534.63 q = 1 T = 21.6°C pH = 7.4

Proton Larmor Frequency(MHz)	Relaxation Rate $(mM \cdot sec)^{-1}$
0.01	14.415
0.02	14.610
0.05	14.327
0.1	13.785
0.2	13.609
0.5	13.184
0.75	12.787
1	12.965
2	12.068
3	11.965
5	10.221
7.5	9.810
10	8.755
15	8.528
20	8.506
30	8.398
40	7.979
50	7.771

Table 6.13

Relaxation Rates of Gd pyrindine-DO3A in 4.5% Human Albumin

M.W. = 534.63 q = 1 T = 21.6°C pH = 7

Proton Larmor Frequency(MHz)	Relaxation Rate(mM•sec)$^{-1}$
0.01	14.148
0.02	15.333
0.05	14.909
0.1	14.831
0.2	15.432
0.5	14.884
0.75	14.723
1	14.318
2	13.881
3	12.992
5	11.775
7.5	10.775
10	10.042
15	9.506
20	9.910
30	9.394
40	9.354
50	8.130

Table 6.14

Relaxation Rates of Gd TTHA in Human Plasma

M.W. = 714.66 q = 0 T = 21.6°C pH = 7.4

Proton Larmor Frequency(MHz)	Relaxaton rates(mM•sec)$^{-1}$
0.01	7.513
0.02	7.550
0.05	7.323
0.1	7.198
0.2	7.010
0.5	6.599
0.75	6.397
1	6.220
2	5.735
3	5.433
5	4.906
7.5	4.488
10	4.153
15	3.787
20	3.569
30	3.375
40	3.265
50	3.223

Table 6.15

Relaxation Rates of Plain Human Plasma at 21.6°C

Proton Larmor Frequency(MHz)	Relaxation Rate$(mM \cdot sec)^{-1}$
0.01	3.026
0.02	3.002
0.05	2.757
0.1	2.591
0.2	2.335
0.5	1.926
0.75	1.725
1	1.602
2	1.266
3	1.091
5	0.923
7.5	0.823
10	0.769
15	0.698
20	0.676
30	0.611
40	0.584
50	0.535

Table 6.16

Relaxation Rates of 5% Human Albumin at 21.6°C

Proton Larmor Frequency(MHz)	Relaxation Rate(mM•sec)$^{-1}$
0.01	1.435
0.02	1.430
0.05	1.417
0.1	1.400
0.2	1.373
0.5	1.291
0.75	1.238
1	1.187
2	0.996
3	0.908
5	0.782
7.5	0.708
10	0.674
15	0.621
20	0.592
30	0.549
40	0.526
50	0.509

Table 6.17

Relaxation Rates of Distilled Water at 20°C

Proton Larmor Frequency(MHz)	Relaxation Rate$(mM \cdot sec)^{-1}$
0.01	0.472
0.02	0.472
0.05	0.471
0.1	0.470
0.2	0.465
0.3	0.463
0.5	0.466
1	0.460
2	0.449
3	0.444
4	0.441
5	0.442
7	0.433
8	0.436
10	0.433
15	0.420
20	0.414
30	0.401
40	0.394
50	0.389

Table 6.18

RESULTS FROM SIMULATIONS OF NMRD CURVES AT 21.6°C

	Solvent	τ_R (psec)	r(Å)	τ_M (nsec)	ZFS$(\frac{2}{3}D^2 + 2E^2)^{\frac{1}{2}}$ (cm^{-1})	q	τ_v (psec)
Gd DOTA	water	72	3.1	9.0	0.015	0.82	4.6
	plasma	78	3.0	36	0.011	0.82	16
Gd DO3A deriv.1	water	77	3.0	8.0	0.036	0.57	7.7
	plasma	79	3.0	18	0.026	0.67	16
Gd DOTA dimer	water	148	3.0	8.1	0.044	0.47	23
	plasma[a)]	330	3.0	30	0.021	0.42	42
Gd(pyridine-DO3A)	plasma[a)]	134	3.0	6.7	0.023	0.96	47

a) This simulation does not count the unbound and the bound Gd complexes separately. Thus the values shown here are the average ones of the two species.

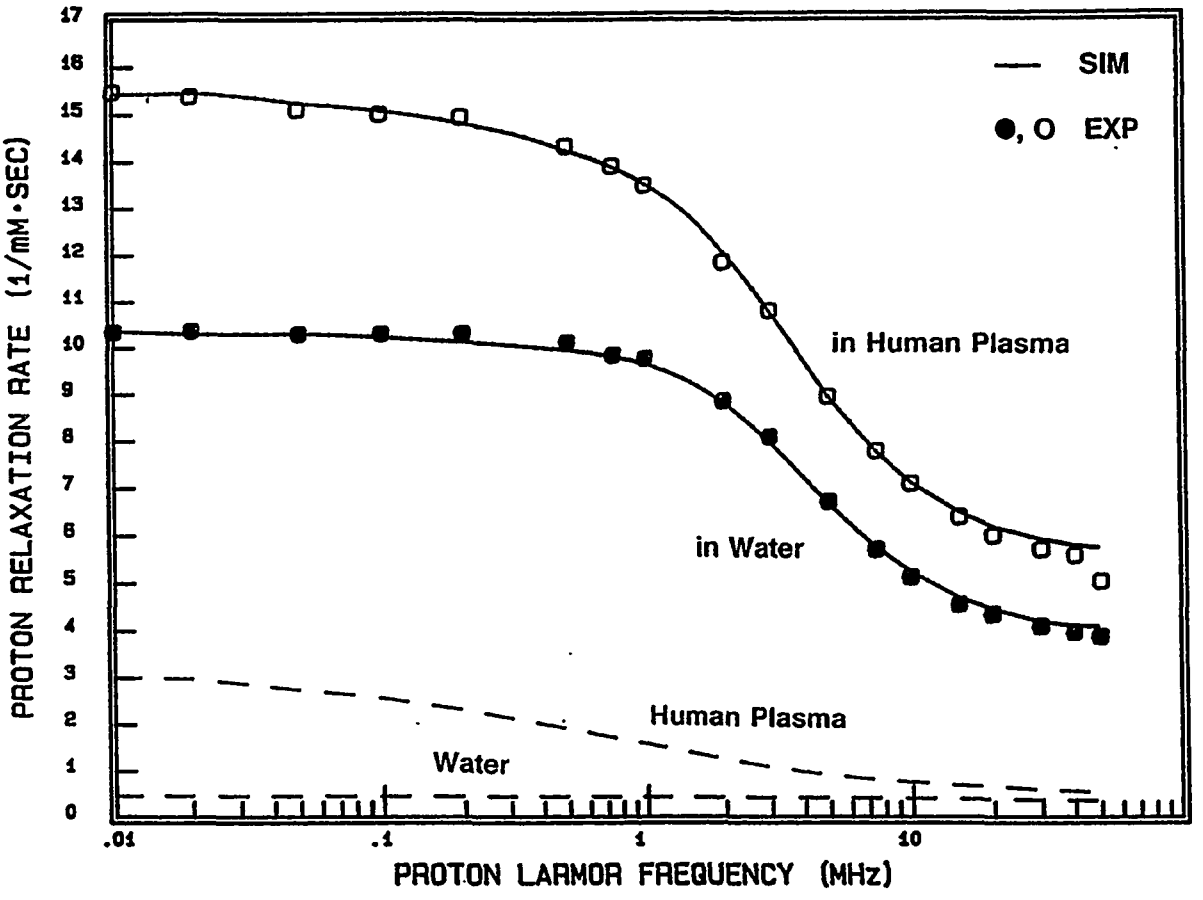

Figure 6.2. Experimetal and Simulated NMRD Profiles of Gd DOTA in Water and Plasma

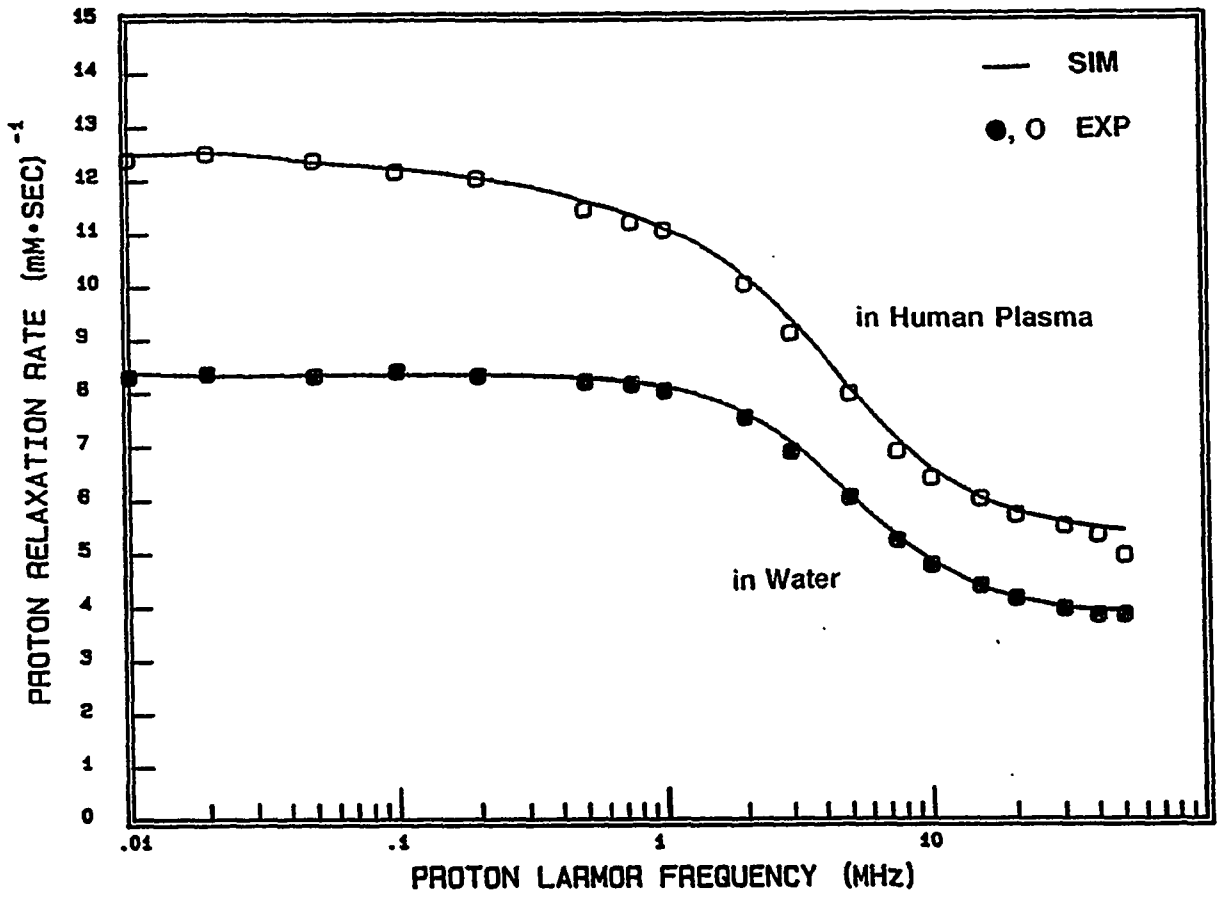

Figure 6.3 Experintal and Simulated NMRD Profiles of Gd DO3A Deriv.1. in Water and Plasma

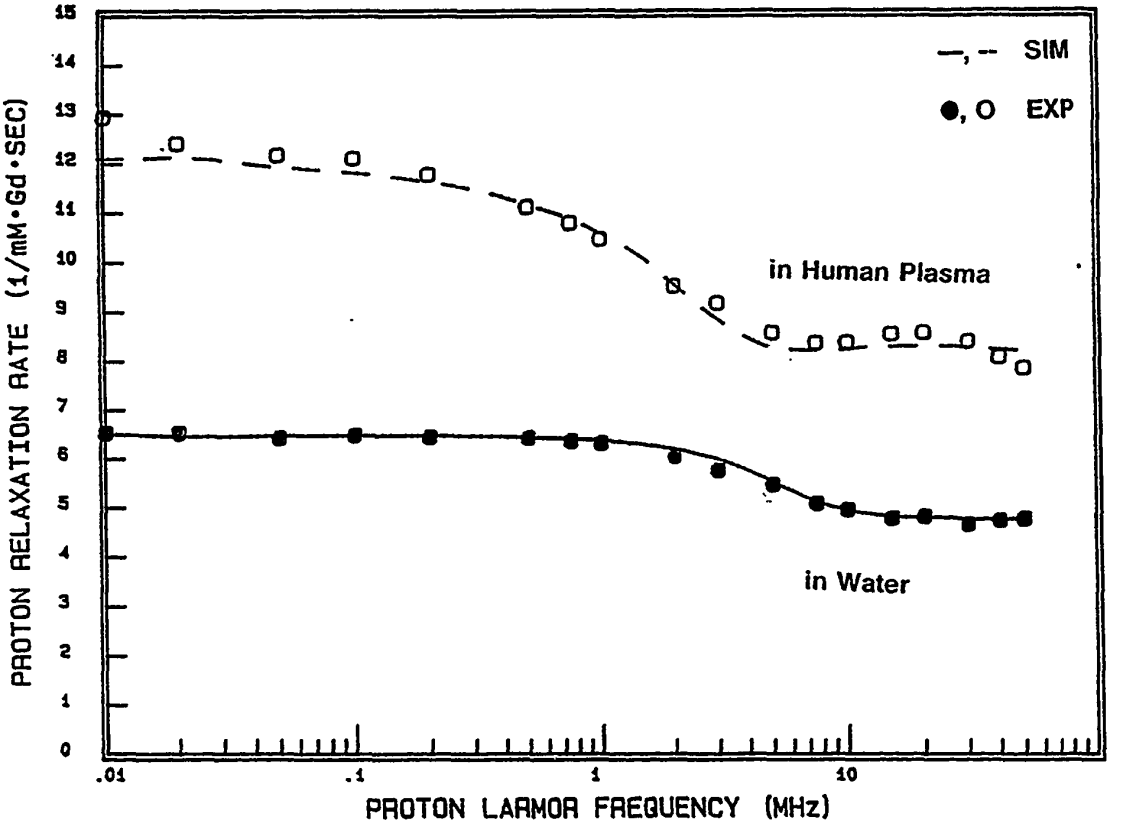

Figure 6.4. Experimental and Simulated NMRD Profiles of Gd DOTA Dimer in Water and Plasma

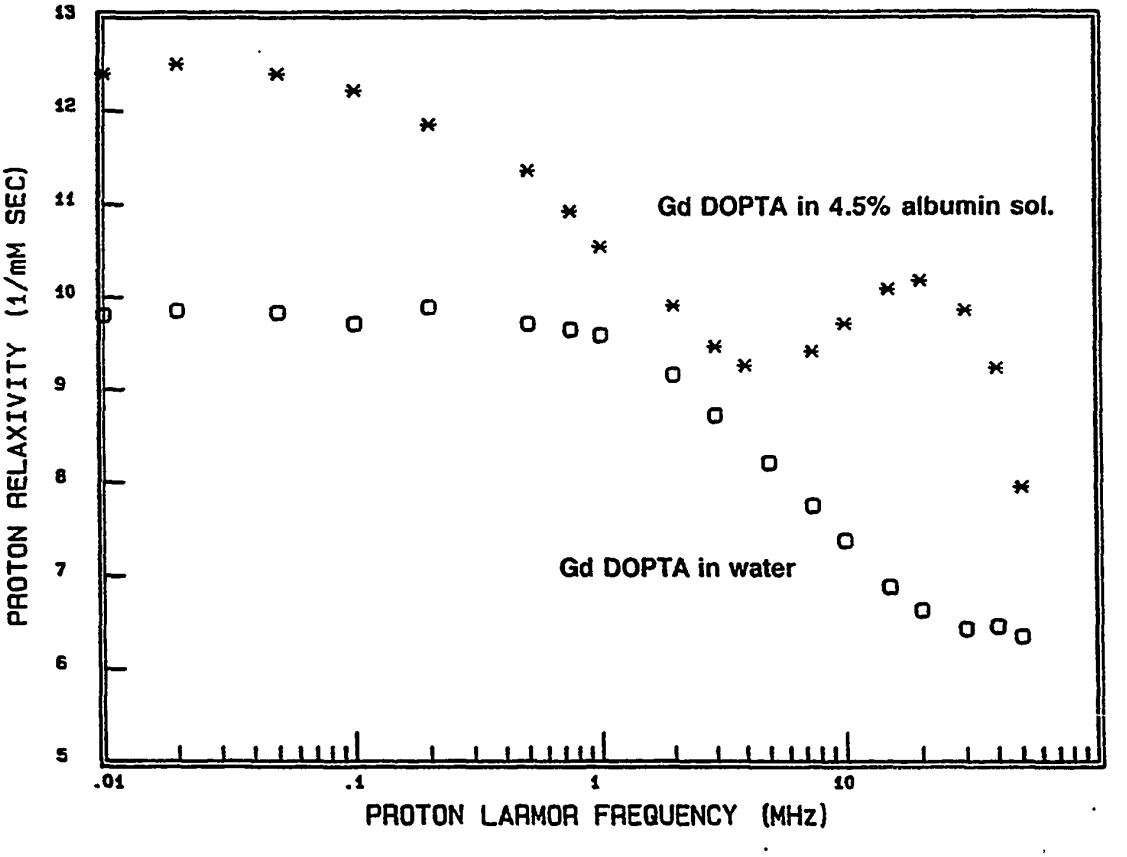

Figure 6.5. Experimental NMRD Profiles of Gd DOPTA in Water and Albumin Sol.

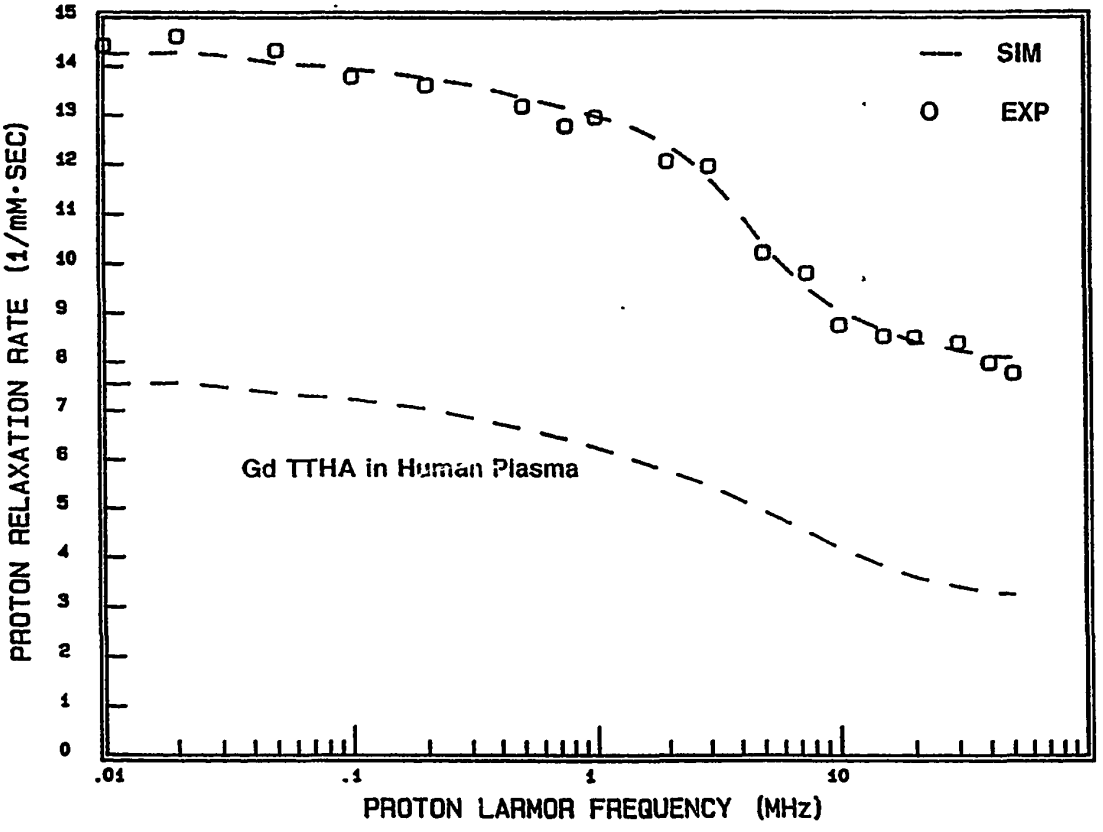

Figure 6.6. Experimental and Simulated NMRD Profiles of Gd (Pyridine-DO3A) in Plasma

REFERENCES

1. Gries,H; Plazek,J.; Raduchel,B.; Renneke,F.-J.; Weinman, H.-J.," the Ninth annual Meeting of Society of Magnetic Resonance in Medicine", 1990, New York

2. Sovak, M., Nucl. Med. Biol., 1988, 15, 3

3. Schmiedl,U.; Ogan, M.; Paajanen, H.; Marotti, M; Crooks, L.E.; Brito, A. C.; Brasch, R. C., Radiology, 1987, 162, 205

4. Padjanen,H.; Reisto, T.; Hemmnila,I.; Komu,M.; Niemi, P.; Kormuno, M., Magn. Reson. Med., 1990, 13, 38

5. Grant, C.W.M.; Karlik, S.; Florio, E., Magn. Reson. Med., 1990, 13, 236

6. Lauffer, R.B.; Detteridge, D.R.; Padmanabhan, S.; Brady, T.J., Nucl. Med. Biol., 1988, 15, 45

7. Larsen, S.K.; Jenkins, B.G.; Memon, N. G.; Lauffer, R.B., Inorg. Chem., 1990, 29, 1147

8. Tweedle, M.K.; Gaugham, G.T.; Hagen,T.; Wedgik, P.K.; Silbery, P.; Wilson, L.J.; Lee, D.W.,Nucl. Med. Biol., 1988, 15, 31

CONCLUDING REMARKS

The goals of this work were i) the physical characterization of factors controlling relaxivity in MRI contrast agents, and ii) investigating new contrast agents by utilizing various characterization methods. A key experiment of this work is NMRD (Nuclear Magnetic Relaxation Dispersion) pioneered by the work of Koenig. Since it is frequently difficult to determine the parameters characterizing relaxivity by NMRD only, complementary spectroscopic studies are very useful. Our approach is to measure the physical properties of Gd-based contrast agents with EPR, Electron Spin Echo (ESE), O-17 NMR, and NMRD, and to develop a set of self-consistent values to fit the key parameters that are believed to control relaxivity. While each of these techniques has been used individually to study contrast agents, the application of all of them to the same system has not been attempted until now. Direct measurements of the factors controlling relaxivity in a series of Gd^{3+} chelates can be shown to correlate well with values from NMRD profiles, even if some experiments were done at low temperature. The results from EPR experiments gave useful information on the zero field splitting values, and ESE experiments provided a good structural picture of the Gd^{3+} solution.

Studies of a new series of Gd-based contrast agents suggested that while the pure hydrophilic complexes did not bind significantly to plasma proteins, some modified complexes did. Non-covalent binding occurred in complexes whose ligands had both hydrophilic and hydrophobic sites. Simulations of NMRD profiles showed substantial increase in the rotational correlation time due to binding to proteins. In conclusion, balancing the hydrophobic and the hydrophilic sites in one molecule can control the binding affinity to plasma proteins according to this work.

VITA

Jong-Hee Hwang was born on June 26, 1956 in Jeonju, South Korea. She received her high School diploma from Ewha Girls' High School. She attended Yonsei University, Seoul Korea, where she earned her B. Eng. degree in Chemical Engineering. She also earned M.S. degree in Chemistry from Yonsei University in 1983. Throughout her graduate career she held numerous teaching assistanceships and research assistanceships. she is a member of the Society of Magnetic Resonance in Medicine.